

Evaluating Security Properties in the Execution of Quantum Circuits

PAOLO BERNARDI, Università di Pisa, Italy

ANTONIO BROGI, Università di Pisa, Italy

GIAN-LUIGI FERRARI, Università di Pisa, Italy

GIUSEPPE BISICCHIA, Università di Pisa, Italy

Quantum computing is a disruptive technology that is expected to offer significant advantages in many critical fields (e.g. drug discovery and cryptography). The security of information processed by such machines is therefore paramount. Currently, modest Noisy Intermediate-Scale Quantum (NISQ) devices are available. The goal of this work is to identify a practical, heuristic methodology to evaluate security properties, such as secrecy and integrity, while using quantum processors owned by potentially untrustworthy providers.

ACM Reference Format:

Paolo Bernardi, Antonio Brogi, Gian-Luigi Ferrari, and Giuseppe Bisicchia. 2025. Evaluating Security Properties in the Execution of Quantum Circuits. 1, 1 (September 2025), 43 pages. <https://doi.org/10.1145/nnnnnnn.nnnnnnn>

Authors' addresses: Paolo Bernardi, paolo@bernardi.cloud, Università di Pisa, Pisa, Italy; Antonio Brogi, antonio.brogi@unipi.it, Università di Pisa, Pisa, Italy; Gian-Luigi Ferrari, gian-luigi.ferrari@unipi.it, Università di Pisa, Pisa, Italy; Giuseppe Bisicchia, giuseppe.bisicchia@phd.unipi.it, Università di Pisa, Pisa, Italy.

Permission to make digital or hard copies of all or part of this work for personal or classroom use is granted without fee provided that copies are not made or distributed for profit or commercial advantage and that copies bear this notice and the full citation on the first page. Copyrights for components of this work owned by others than ACM must be honored. Abstracting with credit is permitted. To copy otherwise, or republish, to post on servers or to redistribute to lists, requires prior specific permission and/or a fee. Request permissions from permissions@acm.org.

© 2025 Association for Computing Machinery.

Manuscript submitted to ACM

Manuscript submitted to ACM

1

CONTENTS

Abstract	1
Contents	2
1 Introduction	4
2 Background: Quantum Circuit Cutting	5
3 Overview of the Approach	6
3.1 Scenario	6
3.2 Threat Model	7
3.3 Objectives	7
3.4 Quantum Circuit Cutting Security Enhancements	8
4 Experimental Validation	10
4.1 Setting the context	10
4.1.1 Test Circuits	10
4.1.2 Test Devices	12
4.1.3 Noise Profile	13
4.1.4 Comparison of Quantum Circuit Evaluation Results	15
4.2 Integrity Testing	16
4.2.1 First test: Raw Circuit Cutting	16
4.2.2 Second Test: Proportional Probability and 2X Replication	16
4.2.3 Third Test: Exponential Probability And 2X Replication	18
4.2.4 Fourth Test: Exponential Probability Without Replication	20
4.2.5 Further tests: Greenberger-Horne-Zeilinger Circuit	22
4.2.6 Further tests: Deutsch-Jozsa Algorithm Circuit	25
4.2.7 Discussion of the Results	27
4.2.8 Proportional VS Exponential Sub-Circuit Allocation Probability	29
4.3 Confidentiality Testing	30
4.3.1 First Test: Raw Circuit Cutting	33
4.3.2 Second Test: 5X Fake Circuits	33
4.3.3 Third Test: 10X Fake Circuits	34
4.3.4 Discussion of the Results	34
4.3.5 Proportional VS Exponential Sub-Circuit Allocation Probability, Revisited	35
4.4 Experimental Methodology Generalization	36
5 Related Work	36
5.1 Integrity Protection	37
5.2 Confidentiality Protection	37
5.3 Noninterference-based Quantum Circuit Security Validation	37
5.4 Positioning of This Work	38
6 Conclusions	38
6.0.1 Goal G1	38
6.0.2 Goal G2	39

Evaluating Security Properties in the Execution of Quantum Circuits	3
6.0.3 Goal G3	39
6.1 Secure Quantum Scheduler	40
6.2 Future Work	41
References	41

1 INTRODUCTION

Quantum computing is rapidly evolving, emphasising its potential across various domains, from cryptography [26] to molecular simulations [1]. Quantum computers are not yet widely available and are typically accessed remotely via cloud-based platforms, which provide computational resources such as quantum emulators, simulators, and experimental Quantum Processing Units (QPUs) over the internet [7, 8, 15, 23]. This cloud-based access is not a limitation; rather, it facilitates effective experimentation and advances in quantum software development. Indeed, cloud-based access enables researchers to experiment with and validate techniques in preparation for more powerful quantum processors. Nonetheless, relying on third-party providers may expose quantum experiments to risks concerning the confidentiality and integrity of the processed information.

In this research context, innovative approaches such as *quantum circuit cutting* [5, 19, 29] offer promising ways to reduce computational demands. By dividing complex quantum circuits into smaller sub-circuits, this technique allows execution on hardware with limited capabilities. While quantum circuit cutting is widely explored for its performance and scalability benefits, there are, to the best of the authors' knowledge, only sparse references to its potential application as a security-enhancing method.

Addressing security concerns in cloud-based quantum computing begins with a clear understanding of the hostile environment and the associated threat model. In this paper, we contextualize the problem by assuming an adversary with both read and write access to subcircuits executed on cloud-connected QPUs. The attacker's objective is either to infer confidential information or to deliberately alter the outcomes of the computation. To devise and evaluate potential countermeasures, we exploit the framework of *probabilistic noninterference* [2] as a guiding principle. This allows us to develop a practical heuristic for comparing the security properties of different quantum circuit cutting security variants, with the goal of identifying the most effective and resilient configurations.

Probabilistic noninterference has been originally introduced to deal with information-flow security for classical and probabilistic systems. Probabilistic noninterference has been shown to be not directly applicable to quantum systems [30], due to two key reasons. First, in quantum systems, information about the state is revealed only through measurement, which inherently disturbs the system and introduces interference between observers. This contrasts with classical or probabilistic systems, where observation does not alter the state. Second, the computational dynamics of quantum systems are governed by unitary operators or super-operators, which differ fundamentally from the stochastic matrices used in classical models. This reflects a distinct mathematical framework for describing agent interactions and system behavior in the quantum realm. Despite its limitations, probabilistic noninterference still provides a valuable conceptual framework to guide our approach, as we will explain below.

The goals of this work are twofold:

- (1) To describe a practical methodology for ensuring confidentiality and integrity when executing quantum circuits within quantum cloud environments;
- (2) To introduce easy-to-apply heuristic measures for the rapid assessment of resilience against confidentiality and integrity breaches, enabling efficient and focused design iterations.

In our research context and experimentation, probabilistic noninterference serves purely as an inspiration for the proposed heuristics. The formal verification of the circuit cutting-based methodology presented in the following sections is beyond the scope of this paper, and it is planned as future work.

The remainder of this paper is organised as follows. Section 2 presents the basic principles of quantum circuit cutting. Section 3 introduces the problem statement (architectural scenario, threat model, goals of the work) and a

set of quantum circuit cutting security enhancements. Section 4 defines the heuristics to measure confidentiality and integrity resilience and applies them to experimentally assess the security enhancements configurations. Section 5 reviews relevant related work while Section 6 concludes the manuscript with a critical discussion of our proposal.

2 BACKGROUND: QUANTUM CIRCUIT CUTTING

Quantum circuit cutting [19] is a technique for the execution of complex quantum circuits over QPUs with a limited number of input qubits, such as current Noisy Intermediate-Scale Quantum (NISQ) [21] devices. The core idea is to split a circuit into smaller sub-circuits with a reduced number of input qubits; the sub-circuits can then be executed in parallel on the available QPUs. To obtain the final result, the partial outputs from the QPUs must be reassembled with a classical post-processing step [5]. Overall, this methodology makes it possible to expand the capabilities of current quantum devices at the cost of an exponentially complex reassembly procedure. Given a quantum circuit cut in k fragments, the reassembly requires $O(16^k)$ time or $O(4^k)$ if the QPUs can communicate with each other [10].

Circuit cutting is commonly performed by analysing and manipulating the circuit's corresponding tensor network [25], a technique adapted from tensor-based quantum simulations. This method offers greater flexibility and a wider range of cutting strategies compared to straightforward qubit partitioning.

The cutting procedure involves a phase that can be summarised in three steps:

- (1) the original quantum circuit is transformed in a tensor network;
- (2) a network edge is cut, resulting in a collection of tensor networks;
- (3) a set of smaller quantum sub-circuits is then derived from the tensor network.

The cutting process can be applied iteratively to ensure that the number of qubits required by each subcircuit aligns with the limitations of the available quantum hardware.

The resulting sub-circuits are distributed to a single QPU one after the other (or to multiple QPUs in parallel [29]), and, finally, their partial outputs are collected.

We already remarked that the post-processing function constructs the global output through classical computation. This step is designed to produce an ϵ approximation of the tensor network result with a 2/3 probability. The post-processing function is defined as follows:

$$f : \{0, 1\}^n \rightarrow [-1, 1].$$

Each cut point in the circuit introduces a virtual qubit, and measurements are performed on multiple bases (such as Pauli bases). The post-processing function combines the results of each sub-circuit with the cut-point measurement outcomes. This algorithm often employs Kronecker products of matrices representing all possible sub-circuit outcomes at each cut point. These aggregated results are then employed to approximate the expectation value of the original quantum circuit.

As the number of cut points increases, so do the configurations to be considered since a new set of bases and their corresponding states are introduced at every cut. In the best case, this post-processing has a $O(4^k)$ time complexity, where k is the number of cuts [10]. This happens because the number of Kronecker products required is 4^k .

Consequently, identifying optimal cut points is crucial, as the search space for a quantum circuit with n edges can grow factorially, up to $O(n!)$. This makes the development of methods for automatic optimal cut-point selection an important area of research in the field [24, 29].

Circuit cutting techniques have been shown to produce acceptable results on several quantum algorithms, ranging from Hamiltonian simulations performed with the Variational Quantum Eigensolver (VQE) algorithm [19] to the Bernstein-Vazirani algorithm [29].

In this paper, we argue that quantum circuit cutting can also serve as a *security countermeasure*: intuitively, by strategically distributing circuit fragments and input data *on multiple QPUs*, no single QPU is ever exposed to the complete circuit, the full input, or the entire computation output. Here, to perform circuit cutting, we leverage the PennyLane framework by Xanadu [4], which offers native support for differentiable quantum circuits and integrates with both software simulators and various QPUs. Specifically, we use its built-in circuit cutting module, which automates the transformation into a tensor graph, the insertion of cut points, and the reconstruction of results. This enables us to focus our experiments on security without being encumbered by low-level implementation details.

3 OVERVIEW OF THE APPROACH

Before presenting the full details of our approach, we first provide an informal overview to highlight its key features and underlying intuition. This high-level summary aims to offer readers a conceptual understanding of the main ideas guiding our methodology.

3.1 Scenario

Quantum computing providers offer Application Programming Interfaces (APIs) that enable cloud-based access to their devices. In this work, we consider a scenario involving a centralized, trusted scheduler – such as the Quantum Broker described in [6] and [8] – which distributes quantum computations to individual QPUs via classical network communication. Throughout the remainder of this paper, we refer to this setup as the *cloud-based quantum computing scenario* (see Figure 1).

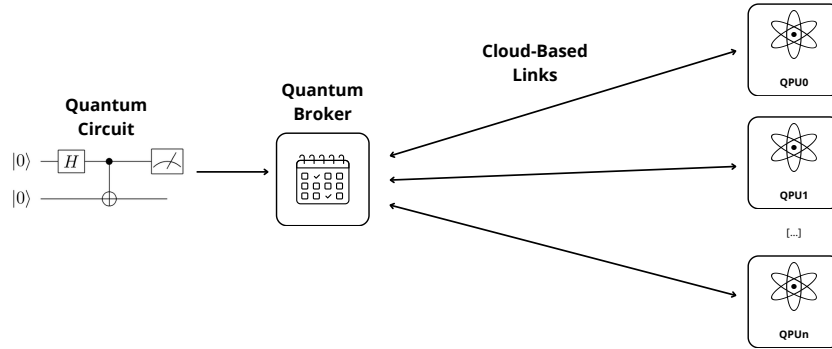


Fig. 1. Graphical representation of the cloud-based quantum computing scenario.

The Quantum Broker can access several QPUs, possibly operated by different vendors. For this reason, we consider a scenario where QPUs, in general, cannot communicate with each other. This setup can be used in combination with Quantum Circuit Cutting to evaluate quantum circuits with a number of input qubits greater than the available NISQ devices capabilities [6]; moreover, distributing circuit fragments across multiple QPUs enables parallel circuit execution.

In this paper, specifically, we consider the following workflow for the execution of a quantum circuit on multiple QPU:

- (1) the Broker splits the original circuit into multiple fragments with a Quantum Circuit Cutting algorithm;
- (2) the Broker sends each fragment to a specific QPU;
- (3) each QPU computes the assigned fragment and produces a partial results;
- (4) the Broker collects the partial results from each QPU;
- (5) finally, the broker combines the partial results with a classical post-processing algorithm to obtain the result of the original circuit.

Therefore, in this scenario, the more QPUs available to the Quantum Broker, the greater the level of parallelism and flexibility. Using more QPUs can decrease the overall execution time, although within limits. The classical post-processing algorithm complexity, in fact, grows with the number of circuit fragments: since we consider a scenario where inter-QPU communication is not guaranteed, the upper bound of the classical post-processing algorithm time is $O(16^k)$, where k is the number of circuit fragments.

In contrast, reducing the number of QPUs available to the Quantum Broker decreases the level of parallelism and flexibility available while reducing the execution time of the post-processing algorithm.

Cybersecurity represents one of the most significant challenges in Quantum Software Engineering (we refer to [18] for a more comprehensive discussion). This paper provides a novel contribution to the field of quantum software security by assessing and enhancing security methodologies that address information security requirements within a cloud-based quantum computing context.

3.2 Threat Model

The considered scenario is characterized by a set of underlying security assumptions briefly explained below.

- (1) There is a trusted central scheduler that distributes quantum circuits and input data to potentially untrusted QPUs and collects their outputs;
- (2) communication links within scheduler and QPUs cannot be trusted;
- (3) the QPUs themselves are potentially untrustworthy.

Figure 2 displays the environment and the trustworthiness of the various actors involved.

The potential objectives of the attackers constitute the basis of the threat model we consider:

- (1) stealing quantum circuits designs, as they could be Intellectual Property (IP) whose development required significant investments;
- (2) stealing quantum computation results;
- (3) disrupting quantum computation results, possibly without detection.

The first two attacker objectives are related to quantum circuits and input data confidentiality, while the third revolves around computation output data integrity.

3.3 Objectives

Our work aims at achieving three main goals:

Goal G1: Given a trusted centralised scheduler and potentially untrusted quantum processors, we propose a methodology aimed at improving the *integrity* of the output data.

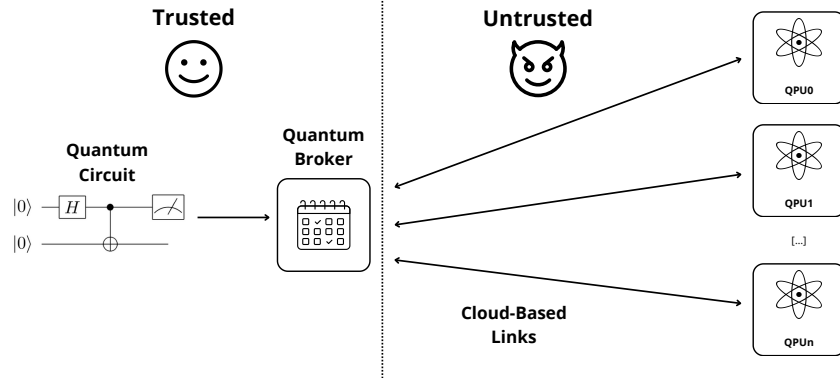


Fig. 2. Graphical representation of the cloud-based quantum computing environment with the range of action of malicious actors.

Goal G2: Given a trusted centralised scheduler and potentially untrusted quantum processors, we propose a methodology aimed at improving the *confidentiality* of algorithms and input/output data.

Goal G3: Provide software engineers with a methodological framework to compare different quantum architectures with respect to integrity and confidentiality resilience.

3.4 Quantum Circuit Cutting Security Enhancements

Plain Quantum Circuit Cutting may offer, as discussed above, some security guarantees concerning integrity and confidentiality. However, to meet our goals, several additional security countermeasures have been added to make cutting more resilient against the threat model.

The countermeasures defined below stem from intuitive considerations. In Section 4, they will be evaluated with a quantitative methodology to experimentally determine local maxima with respect to integrity and confidentiality resilience. Our evaluation framework could also be used by system designers to explore secure architecture alternatives.

Enhancement	Target	Description	Rationale
i1. Dynamic QPU integrity score	Integrity	Probe circuits with known expectation values are sent to QPUs to evaluate how their computations differ from the ground truth. An <i>integrity score</i> is then evaluated (see Equation 2). The integrity score is meant to be directly proportional to a QPU integrity resilience.	The integrity score is not a countermeasure per se, but it is a prerequisite for integrity protection techniques: being able to compare how well each QPU preserves integrity allows for targeted circuit fragment allocation.
i2. Probabilistic sub-circuit assignment	Integrity	Sub-circuits are assigned to each QPU in a probabilistic fashion, depending on its integrity score. In Subsection 4.2, two probability computation criteria (proportional and exponential) are evaluated.	Intuitively, allocating more circuit fragments to the most reliable QPUs, while tending to avoid the least reliable ones, should enhance the overall resilience against integrity attacks.
i3. Sub-circuit replication	Integrity	Sub-circuits are evaluated by more than one QPU, depending on a <i>replication factor</i> , and their results are averaged using the QPUs's integrity scores as weights.	Having circuit fragments evaluated by more than one QPU, and combining their results by weighing them according to their integrity score, can help mitigate the effect of unreliable QPUs. This approach differs slightly from <i>i2. Probabilistic QPU assignment</i> : rather than avoiding problematic QPUs, it allows them to participate in the computation while reducing the impact of their results.
c1. Fake sub-circuits	Confidentiality	Fake sub-circuits are mixed with real sub-circuits to make it harder for QPUs to detect the actual computation being performed.	Mixing fake circuit fragments with real ones makes it harder for compromised QPUs to infer sensitive data or reverse-engineer the original quantum circuit.

Table 1. Quantum Circuit Cutting security enhancements

The integrity score, based on the results of probe circuits evaluation by each QPU, is as follows:

$$error = expected_result - actual_result, \quad (1)$$

$$integrity_score = \max(0, 10 - \frac{error}{expected_result} \cdot 10). \quad (2)$$

Each probe circuit is characterised by a known expectation value. To assess the integrity resilience of a QPU, we firstly compute the difference between this theoretical value and the actual result produced by the device. This difference, referred to as the *error*, reflects the deviation from the expected result: the higher the error, the less reliable the QPU is considered. Finally, the QPU integrity score is derived by normalising the error within a predefined range (in this example 0 to 10), so that a higher integrity score corresponds to greater QPU reliability.

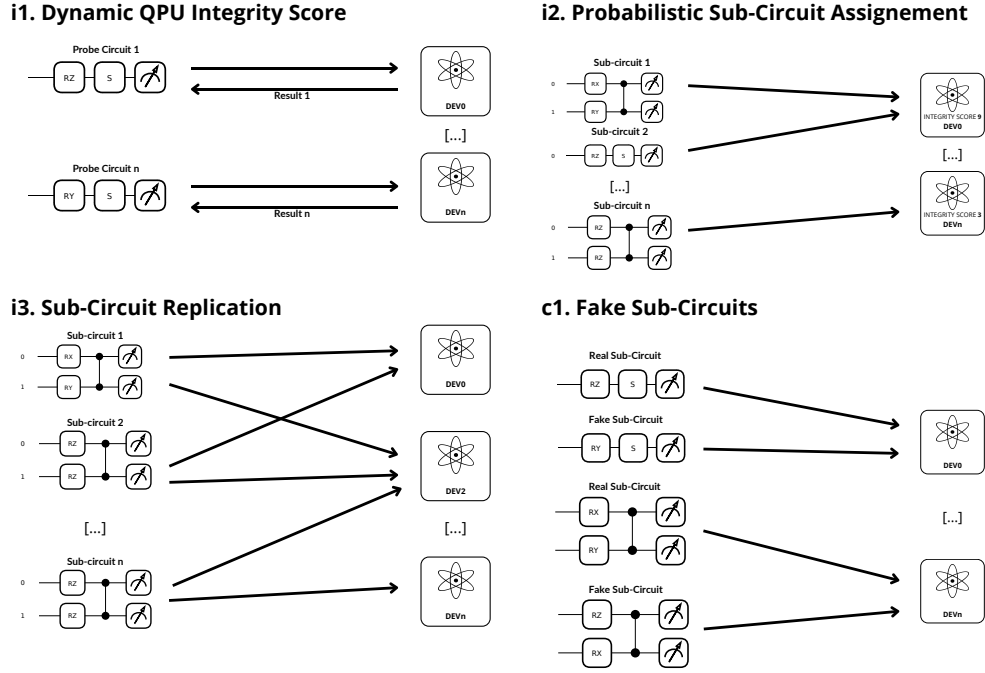


Fig. 3. Graphical representation of countermeasures for circuit cutting integrity and confidentiality resilience.

4 EXPERIMENTAL VALIDATION

In this section, we illustrate the steps of the evaluation procedure designed to assess the extent to which the concept of circuit cutting can function as an effective security countermeasure against adversarial attacks, within the framework of cloud-based access to quantum computing devices.

We begin by outlining the key features of the testing methodology adopted in our approach. This includes a detailed description of the underlying assumptions: circuits, tools and test environment. We then move to illustrate the criteria used to assess the effectiveness of the security countermeasure. By clarifying these aspects, we aim to provide a transparent and reproducible basis for interpreting the obtained results.

4.1 Setting the context

4.1.1 Test Circuits. The quantum circuits used in the experimental setting include standard algorithms, such as Greenberger-Horne-Zeilinger (GHZ) and Deutsche-Jozsa, and custom quantum circuits specifically developed for the purposes of this evaluation activity.

Firstly, standard quantum algorithms are employed to ensure relevance to practical real-world applications. Secondly, custom circuits with uniform structures and distinct gate patterns are employed to probe specific behavioural characteristics of quantum devices that may not be fully captured by standard circuits. To this end, our custom circuits incorporate

seemingly random elements and regular, algorithmic structures. This dual approach enables a more comprehensive evaluation of the methodology across a broader range of quantum computational scenarios.

Our first custom benchmark circuit, displayed in Figure 4, utilizes 15 qubits and it is employed in integrity-resilience experiments. The first six qubits are initialized by combining rotations along the X and Y axes of the Bloch sphere through RX and RY gates. Each qubit is rotated by a specific angle.

Subsequently, qubits are linked with CZ gates by applying a phase flip that depends on the respective control qubits. Then, the first four qubits are further processed with RX and RY gates. Finally, two cut points are added on wires 1 and 3 as a prerequisite for quantum circuit cutting. Up to the tenth, the remaining qubits are rotated and phase flipped using the RX, RY, and CZ gates.

The gates that act on the remaining qubits are generated algorithmically. Each qubit (from the eleventh to the fifteenth) has a rotation RX and a RY proportional to its index, and it is phase-flipped by using the previous qubit as control.

The measurement consists of a Pauli-Z on each qubit combined with a Kronecker product, as shown in equation 3:

$$Z_0 \otimes Z_1 \otimes Z_2 \otimes Z_3 \otimes \cdots \otimes Z_{14}. \quad (3)$$

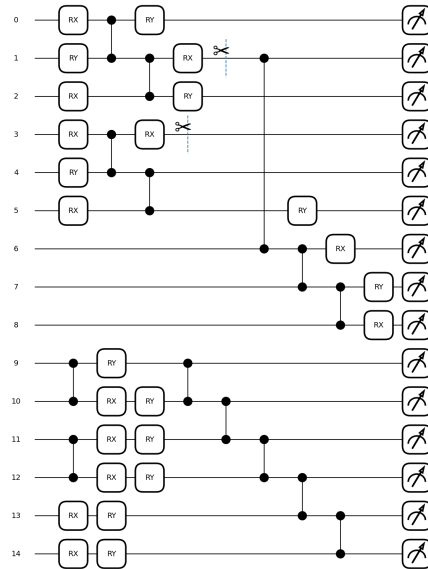


Fig. 4. Graphical representation of the 15 qubit quantum circuit used to perform the experiments.

The expectation values for the benchmark circuit follow a Gaussian distribution described by the parameters $\mu = 0.001013413$ and $\sigma = 0.000000282$. Figure 5a shows the histogram of the expectation values derived with an experiment of 5000 circuit evaluations (5000 shots each), while Figure 5b displays the box plot diagram of the expectation values.

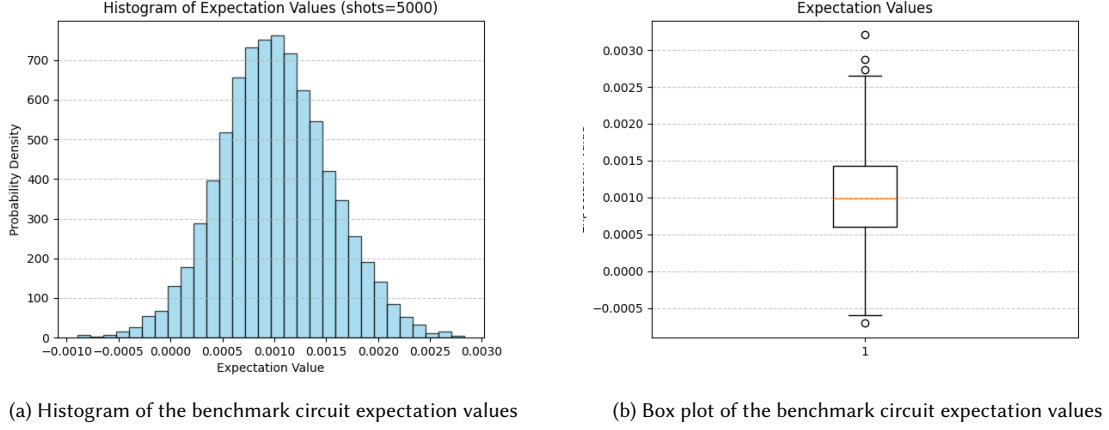


Fig. 5. Graphical analysis of the benchmark circuit expectation values

Furthermore, we designed a second custom circuit for confidentiality testing, referred as the alternative benchmark circuit. Compared to the first one, it is structurally simpler but it has a larger percentage of noisy gates.

Figure 6 shows the second custom circuit structure. While the gates are different from the first custom benchmark circuit, it is still a 15 qubit circuit, and the measurements consist of Pauli-Z observables on each qubit combined with a Kronecker product as well:

$$Z_0 \otimes Z_1 \otimes Z_2 \otimes Z_3 \otimes \cdots \otimes Z_{14}. \quad (4)$$

The alternative benchmark circuit expectation values follow a Gaussian distribution described by the parameters $\mu = 0.005726323$ and $\sigma = 0.000000327$. Figure 7a shows the histogram of the expectation values derived via an experiment of 5000 circuit evaluations with 5000 shots each, while Figure 7b displays the box plot diagram of the expectation values.

4.1.2 Test Devices. The availability of cloud-accessible NISQ quantum processors from commercial vendors marks a significant milestone in the development and practical understanding of quantum computing. These quantum devices can be accessed through software libraries such as Qiskit [14], which interface with the hardware via a custom token-based HTTP API. However, current QPUs are not yet practical in a context where running hundreds or thousands of tests is required, since free-tiers have strict usage time accounting and non-free hardware access is considerably expensive.

Therefore, the following experiments have been performed on software-based noisy QPU simulators. The test QPUs used in this work consist of six Qiskit Aer simulators (see Figure 8). The flexibility of Qiskit Aer made it possible to perform experiments both Intel CPUs and NVIDIA GPUs. The devices were configured to support 15 qubits, matching the input size of the circuits used in the experiments. This specific input size has been chosen as a trade-off between meaningful computational input and test execution time.

Depending on the specific testing requirements, the test devices run in two different ways:

- (1) **Reliable:** the simulated QPU returns the actual *true* computation result.
- (2) **Malicious:** the QPU alters the output result up to 250%. The actual magnitude of the attack is defined probabilistically through a Random Number Generator (RNG) with a configurable seed value. Specifically, given the i^{th}

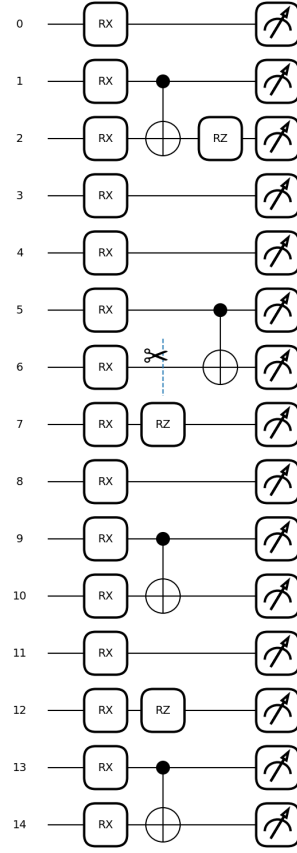


Fig. 6. Graphical representation of the alternative 15 qubit quantum circuit used to perform confidentiality experiments together with the original benchmark circuit, GHZ and Deutsch-Jozsa

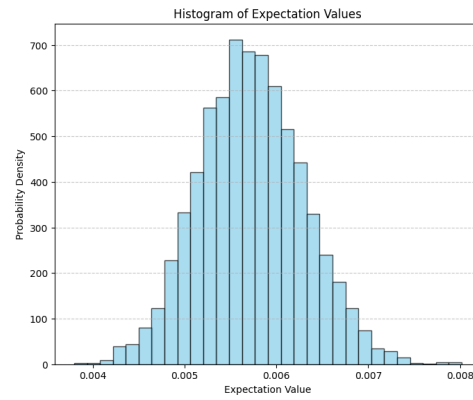
result of the n^{th} QPU, the result is altered as follows:

$$res_{n,i} = (1.5 + r)res_{n,i},$$

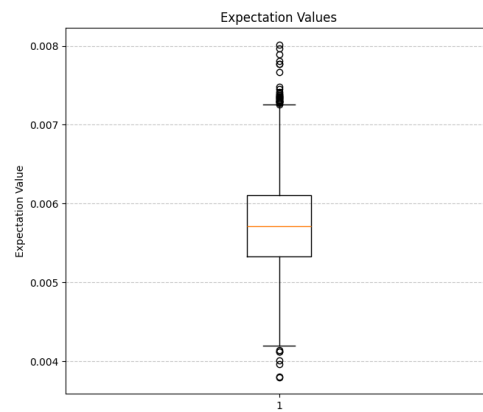
where r is a random number in the $[0, 1)$ range.

4.1.3 Noise Profile. The noise profile used for the experiments involves only three gates: RX , RY , and $CNOT$. Their behaviour is altered as follows:

- RX and RY gates are subject to thermal relaxation errors with 2% and 1.5% probability respectively. This error simulates the decoherence caused by the interaction with the environment, given by the parameters T_1 ($50\mu s$, the average relaxation time toward the $|0\rangle$ state) and T_2 ($30\mu s$, the average dephasing time). The density matrix evolution is characterized by a combination of T_1 exponential decay and T_2 decoherence.



(a) Histogram of the alternative benchmark circuit expectation values



(b) Box plot of the alternative benchmark circuit expectation values

Fig. 7. Graphical analysis of the alternative benchmark circuit expectation values

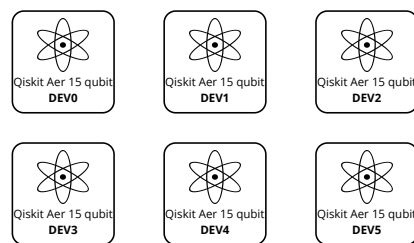


Fig. 8. Simulated devices used to perform the experiments

Listing 1. *Noise model*

```

cnot_error = depolarizing_error(0.01, 2)
rx_error = thermal_relaxation_error(50e-6, 30e-6, 0.02)
ry_error = thermal_relaxation_error(50e-6, 30e-6, 0.015)
noise_model.add_all_qubit_quantum_error(cnot_error, ['cx'])
noise_model.add_all_qubit_quantum_error(rx_error, ['rx'])
noise_model.add_all_qubit_quantum_error(ry_error, ['ry'])

```

- The *CNOT* gate is subject to depolarisation, a random noise that affects the whole quantum state space. This error simulates hardware errors due to qubit instability or external interference. The following formula describes the depolarisation error effects on the density matrix:

$$\mathcal{E}(\rho) = (1 - p)\rho + \frac{p}{d}I,$$

where ρ is the initial density matrix, p is the depolarization probability, d is the system size (e.g. $d = 4$ for a two-qubit system), and I is the identity matrix.

The Qiskit API exposes simulated devices, such as Fake127QPulseV1, a 127 qubit processor with a complex topology inspired by IBM's Eagle QPUs. This model allows for fine-grained parameter control for pulse-level simulation, including pulse duration and shape. Additional customisable parameters decoherence times for each qubit, reading error probability, gate error rates, and inter-qubit links.

In our tests we applied the noise profile defined above to a Fake127QPulseV1 simulated device. This specific device was selected since it mimics the topology of real-world devices, while the noise profile was defined to ensure controlled and interpretable evaluation conditions. The selected gates, *RX*, *RY*, and *CNOT*, are the most common gates used in our testing circuits. Applying thermal relaxation to single-qubit rotations reflects realistic decoherence phenomena common in superconducting quantum hardware. The depolarising noise applied to the *CNOT* gate, instead, captures the probabilistic nature of multi-qubit gate failures, which are typically the most error-prone operations in NISQ devices. This specific noise setup provides a simplified, easy to interpret, yet meaningful abstraction of typical noise sources.

4.1.4 Comparison of Quantum Circuit Evaluation Results. The experiments to validate integrity and confidentiality resilience of Quantum Circuit Cutting-based schemes depend crucially on comparing the output probability distributions of the benchmark quantum circuits.

To compare probability distributions we employ Hellinger Distance, as it is customary in the quantum computing field [3, 12, 17, 20]:

$$H(P, Q) = \frac{1}{\sqrt{2}} \sqrt{\sum_{x \in \mathcal{X}} \left(\sqrt{P(x)} - \sqrt{Q(x)} \right)^2}, \quad (5)$$

Hellinger Distance varies from 0 (the probability distributions P and Q are exactly the same) to 1 (they are completely different).

In the experimental results analysis, we will consider two distributions to be sufficiently similar if their Hellinger distance is at most 0.25. This threshold was determined considering two factors:

- (1) **Distribution overlap:** considering the relationship between Hellinger distance and Total Variation Distance (TVD) defined above, for a Hellinger distance threshold of 0.25, the TVD is at most 0.35, which means that almost two thirds of the distributions do not overlap.
- (2) **Bayes error probability** for a Hellinger distance threshold of 0.25, the corresponding Bayes error probability is approximately 1.5%. Therefore, a classifier trying to distinguish between two distributions having this threshold would have a considerably low error probability.

4.2 Integrity Testing

In order to quantify the degree of integrity protection guaranteed by Quantum Circuit Cutting, and to compare the effectiveness of the additional countermeasures defined in Subsection 3.4, we define an heuristic framework inspired by Probabilistic Noninterference (PNI).

We begin by dividing output data in two categories:

O_{hi} is the high-level output that malicious QPUs are trying to subvert;

O_{lo} is the low-level output produced by well behaving QPUs;

$O_{lo'}$ is the low-level output produced by malicious QPUs;

If an integrity-preserving procedure guarantees integrity, then the following probabilistic relationship should be verified:

$$P(O_{hi}|O_{lo}) \simeq P(O_{hi}|O_{lo'}), \quad (6)$$

This means that partial outputs from malicious QPUs should not alter the overall computation output.

In our experimental assessment, we employed the following procedure to practically verify the validity of Equation 6:

- (1) Compute the probability distribution of the benchmark circuit output (*ground truth*);
- (2) Compute the Hellinger distance between the ground truth and the distribution produced by a system where 1 QPU is acting maliciously, by altering its output O_{lo} ;
- (3) Add one malicious QPU (so now there are two attackers) and measure the distance from ground truth again;
- (4) Repeat step 3 until all 6 QPUs are acting maliciously.

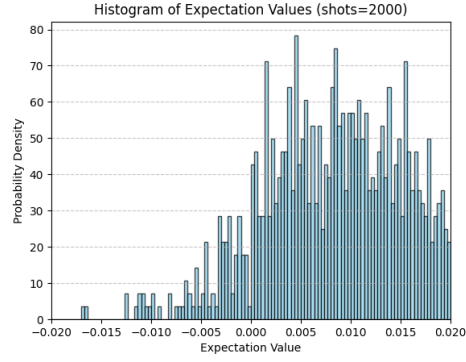
As specified in subsection 4.1, attacking QPUs can alter their O_{lo} values by up to 250%.

In the following sections, guided by the principles of PNI we test combinations of the proposed security enhancement techniques on different circuits and with an increasing number of malicious QPUs (i.e. saboteurs) and measure how they improve the integrity of the overall quantum computation.

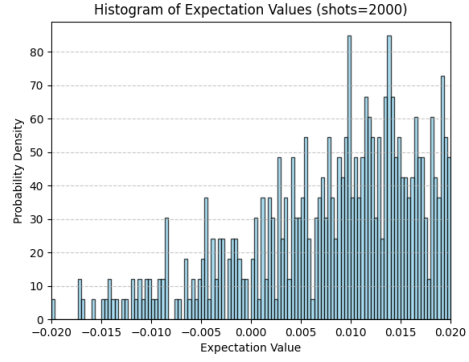
4.2.1 First test: Raw Circuit Cutting. Firstly, the impact of attacking QPUs was evaluated over plain quantum circuit cutting without any additional protection.

As shown in the histograms in Figure 9 and by the variations on the Hellinger distance from the ground truth displayed in Figure 10 and Table 2, even a single saboteur has a significant impact on the overall result, making it markedly different from the reference values. In other words, without the introduction of suitable countermeasures (see Section 3.4) circuit cutting is not resilient against active attackers that compromise data integrity. Therefore, the subsequent tests will focus on enhancing integrity resilience through the application of several protective countermeasures.

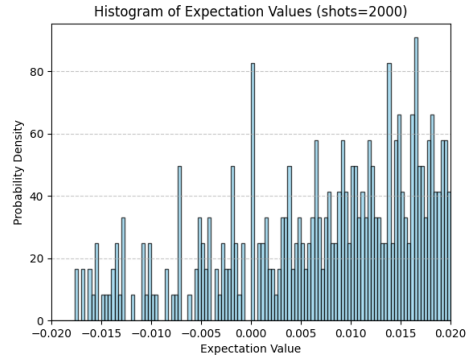
4.2.2 Second Test: Proportional Probability and 2X Replication. In the second batch of tests, the sub-circuits, replicated twice, are distributed among the QPUs with a probability proportional to their *integrity score* IS_n computed with probe circuits, as described in Section 3.4. The probability P_n of selecting the n^{th} QPU is computed as follows:



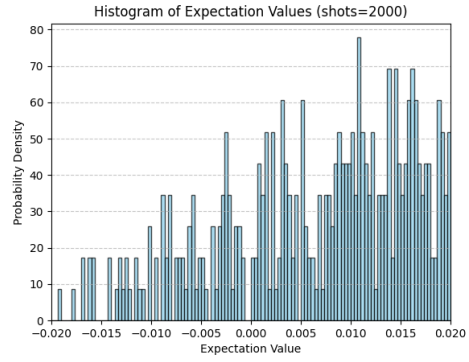
(a) One saboteur



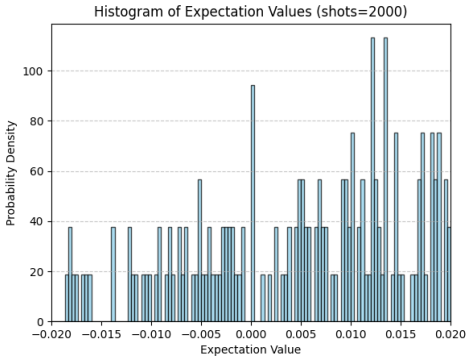
(b) Two saboteurs



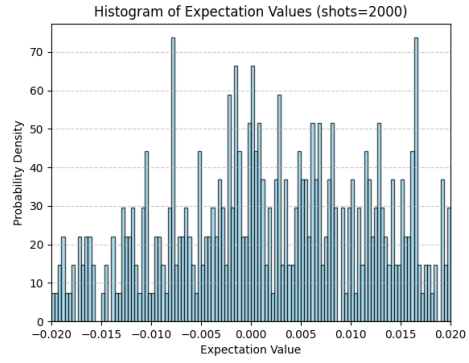
(c) Three saboteurs



(d) Four saboteurs



(e) Five saboteurs



(f) Six saboteurs

Fig. 9. Integrity evaluation with a progressively larger amount of saboteurs and an unprotected circuit cutting algorithm.

Attackers	Distance From Ground Truth
0	0
1	0.785
2	0.849
3	0.857
4	0.833
5	0.913
6	0.788

Table 2. Hellinger distance from ground truth with a growing number of attacking QPUs and with unprotected circuit cutting.

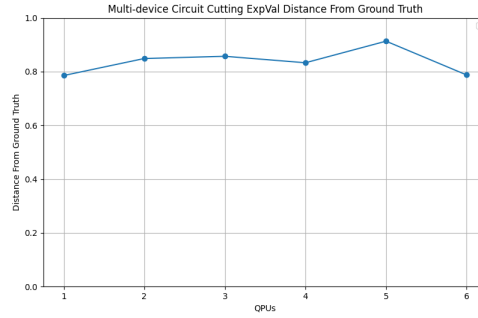


Fig. 10. Hellinger distance from ground truth with a growing number of integrity saboteurs and an unprotected circuit cutting algorithm.

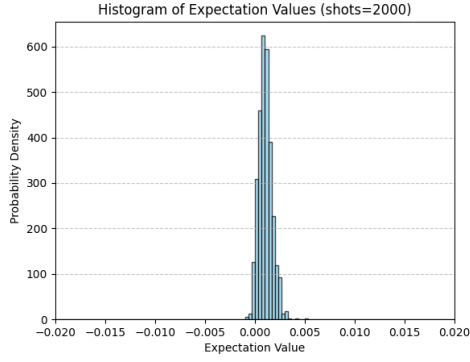
$$\frac{IS_n}{\sum_{i=0}^5 IS_i}. \quad (7)$$

Figure 11 displays the high-level output probability distributions as the number of saboteurs increases (from 1 to 6). While a single saboteur does not significantly alter the overall distribution shape, the test involving six saboteurs results in a significantly different distribution.

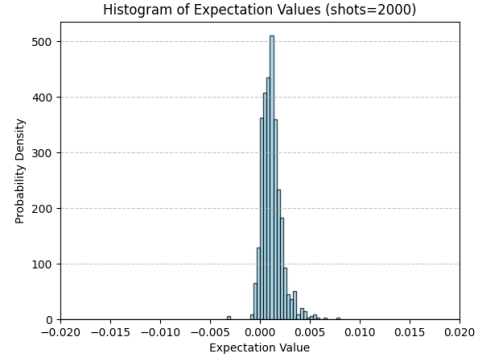
This visual result can be quantitatively assessed by measuring the Hellinger distance between each distribution and the ground truth. As shown in Figure 12, the presence of up to three saboteurs among the six QPUs does not significantly alter the outcome. However, from four to six saboteurs, the distance from the ground truth increases incrementally, approaching a value of 1.

4.2.3 Third Test: Exponential Probability And 2X Replication. In the third round of testing, the probability of assigning sub-circuits to the QPUs was modified from being linearly proportional to being exponentially dependent on the *integrity score* IS_n . Meanwhile, the replication factor was kept constant at 2X. The updated formula that determines which QPU will be used to execute quantum sub-circuits is as follows:

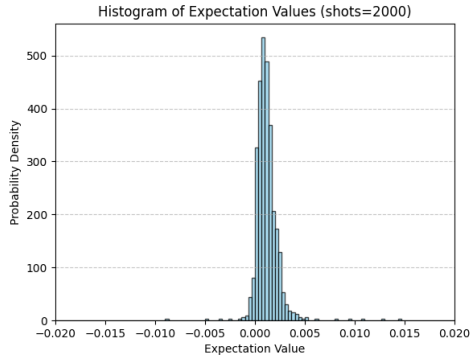
$$\frac{e^{IS_n}}{\sum_{i=0}^5 e^{IS_i}}. \quad (8)$$



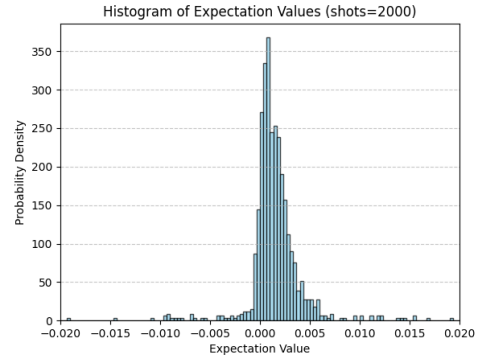
(a) One saboteur



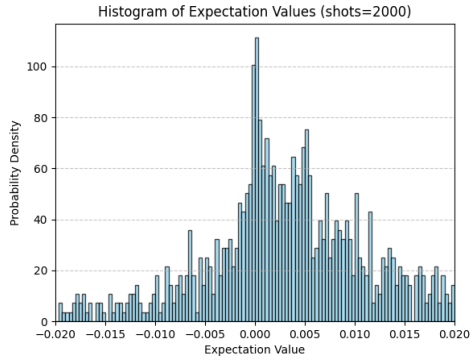
(b) Two saboteurs



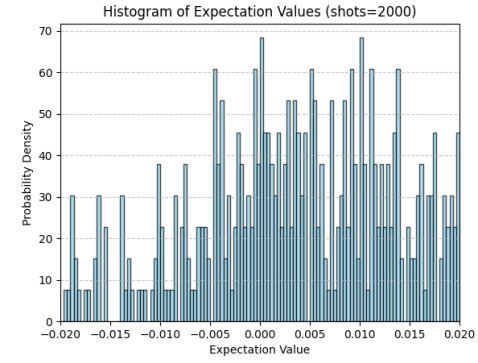
(c) Three saboteurs



(d) Four saboteurs



(e) Five saboteurs



(f) Six saboteurs

Fig. 11. Integrity evaluation with a progressively larger amount of saboteurs and with an execution probability proportional to the QPU integrity score and a 2X replication factor.

Attackers	Distance From Ground Truth
0	0
1	0.092
2	0.210
3	0.184
4	0.384
5	0.745
6	0.807

Table 3. Hellinger distance from ground truth with a growing number of attacking QPUs, with an execution probability proportional to the QPU integrity score and with a 2X replication factor

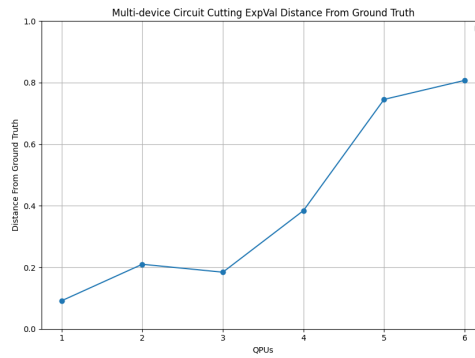


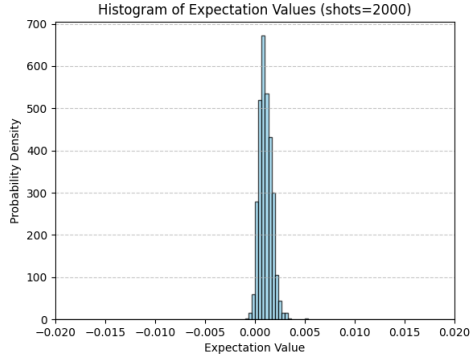
Fig. 12. Hellinger distance from ground truth with a growing number of integrity saboteurs with an execution probability proportional to the QPU integrity score and a 2X replication factor

This assignment criterion shifts most of the workload to the most reliable QPUs while under-utilizing suspicious processors. Figure 13 displays the high-level output probability distributions with a growing number of saboteurs (from 1 to 6) and an exponential probability of sub-circuit execution.

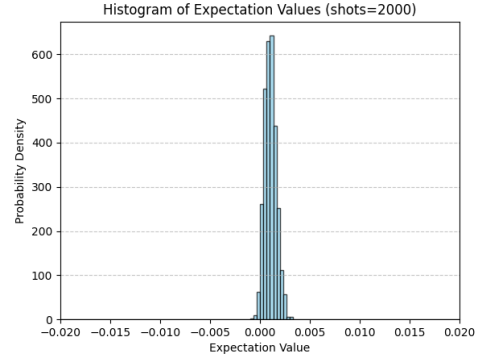
This visual result can be quantitatively assessed by measuring the Hellinger distance between each distribution and the ground truth. As shown in Figure 14 and Table 4, the presence of up to four saboteurs among the six QPUs does not significantly alter the outcome. However, the distance increases sharply from five to six saboteurs, approaching a value of 1. This represents a clear improvement over the previous test, in which the assignment probability was linearly proportional to the QPU integrity score.

4.2.4 Fourth Test: Exponential Probability Without Replication. Introducing exponential replication probabilities led to an improvement in integrity resilience; therefore, we will retain this probability criterion. We now proceed to evaluate the benchmark circuit *without sub-circuit replication*. The probability model for sub-circuit distribution remains exponential with respect to the integrity score.

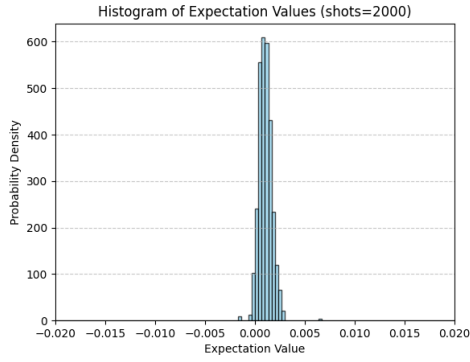
As shown in Table 5, this configuration yields the best possible result: the distance from the ground truth remains low with up to five saboteurs (i.e., even if more than the half of our actors are malicious), with the only significantly altered outcome occurring when all six QPUs are compromised.



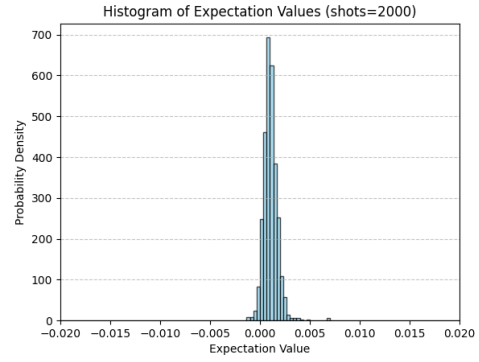
(a) One saboteur



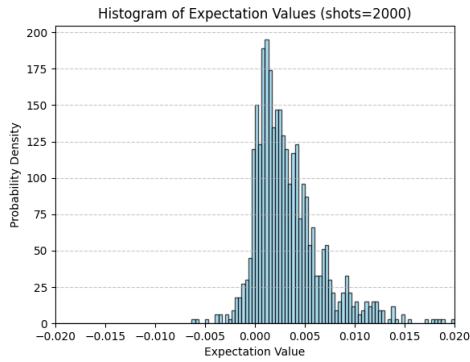
(b) Two saboteurs



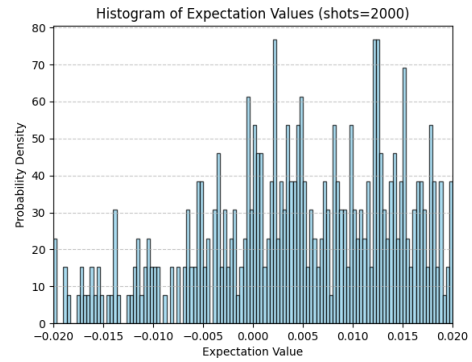
(c) Three saboteurs



(d) Four saboteurs



(e) Five saboteurs



(f) Six saboteurs

Fig. 13. Integrity evaluation with a progressively larger amount of saboteurs with an execution probability exponential with respect to the QPU integrity score and a 2X replication factor.

Attackers	Distance From Ground Truth
0	0
1	0.077
2	0.063
3	0.074
4	0.080
5	0.572
6	0.817

Table 4. Hellinger distance from ground truth with a growing number of attacking QPUs, with an execution probability exponential with respect to the QPU integrity score and a 2X replication factor.

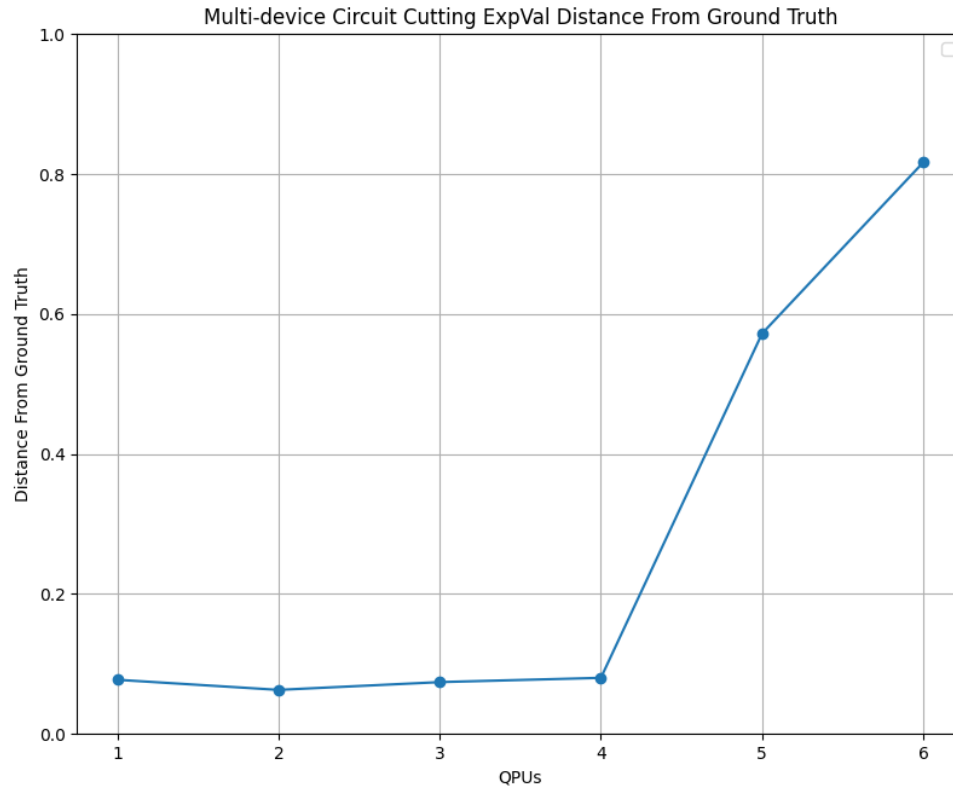
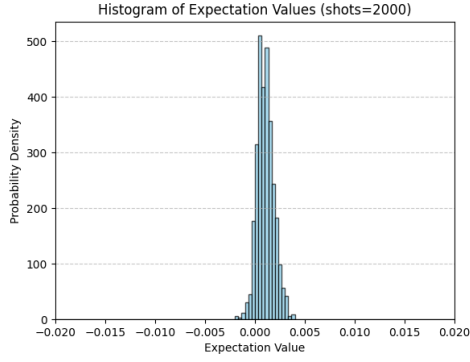
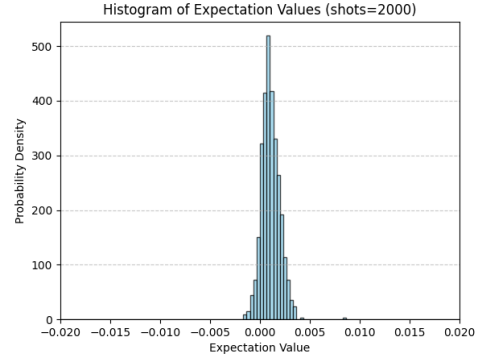


Fig. 14. Hellinger distance from ground truth with a growing number of integrity saboteurs with an execution probability exponential with respect to the QPU integrity score and a 2X replication factor.

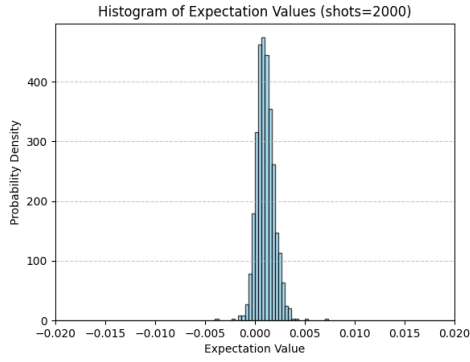
4.2.5 Further tests: Greenberger-Horne-Zeilinger Circuit. The GHZ circuit is used to create an entangled, highly-correlated state [13]. The GHZ state is a generalization of the Bell state for more than two qubits, and it is a cornerstone



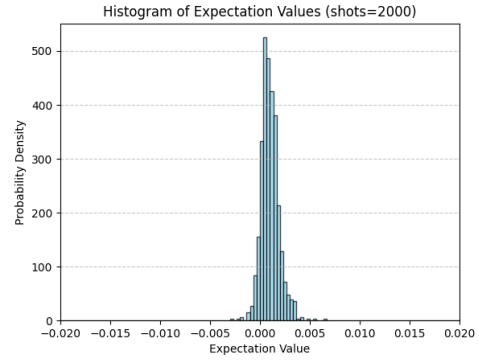
(a) One saboteur



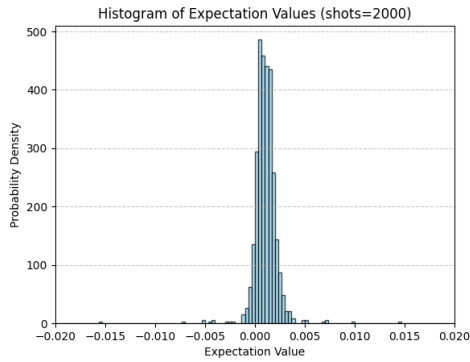
(b) Two saboteurs



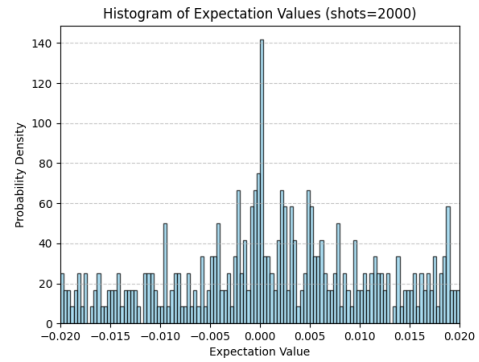
(c) Three saboteurs



(d) Four saboteurs



(e) Five saboteurs



(f) Six saboteurs

Fig. 15. Integrity evaluation with a progressively larger amount of saboteurs with an execution probability exponential with respect to the QPU integrity score and without sub-circuit replication.

Attackers	Distance From Ground Truth
0	0
1	0.080
2	0.068
3	0.077
4	0.098
5	0.114
6	0.752

Table 5. Hellinger distance from ground truth with a growing number of attacking QPUs, with an execution probability exponential with respect to the QPU integrity score and without sub-circuit replication.

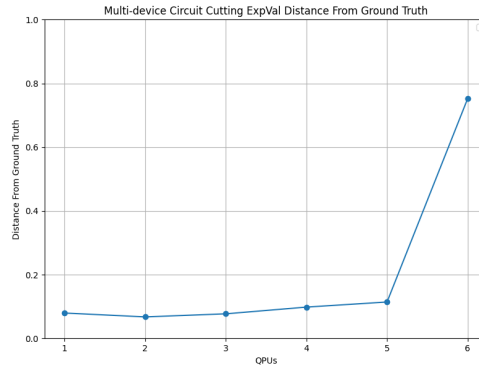


Fig. 16. Hellinger distance from ground truth with a growing number of integrity saboteurs with an execution probability exponential with respect to the QPU integrity score and without sub-circuit replication.

example in entanglement and non-local quantum phenomena. For example, in a three-qubit system, the GHZ state is defined as follows:

$$|GHZ\rangle = \frac{1}{\sqrt{2}}(|000\rangle + |111\rangle).$$

The GHZ circuit generates the corresponding state with a combination of quantum gates. For example, in the case of three qubits, the circuit structure is the following:

- (1) apply a Hadamard gate to the first qubit to create a $|0\rangle + |1\rangle$ quantum superposition: $H|0\rangle = \frac{1}{\sqrt{2}}(|0\rangle + |1\rangle)$;
- (2) apply two *CNOT* gates, the first using the first qubit as control and the second qubit as target, the second using the first qubit as control and the third as target.

Figure 17 depicts this circuit with a three qubit input.

The same tests conducted on the benchmark circuit were also performed on a 15-qubit GHZ circuit from the Munich Quantum Toolkit (MQT) benchmark suite [22] (with two circuit cuts applied):

- (1) raw circuit cutting;
- (2) proportional sub-circuit allocation probability and 2X replication;

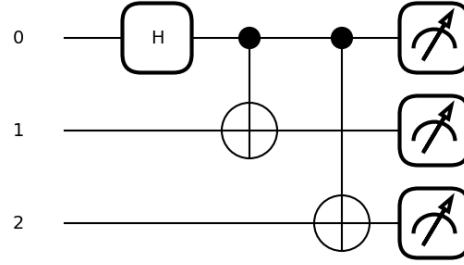


Fig. 17. Three qubit GHZ circuit.

- (3) exponential sub-circuit allocation probability and 2X replication;
- (4) exponential sub-circuit allocation probability and 3X replication;
- (5) exponential sub-circuit allocation probability without replication.

The tests were performed with a growing number of attacking QPUs, ranging from 1 to 6, and the corresponding distribution of expectation values was compared to the ground truth (the circuit executed without any compromised QPU) with the Hellinger Distance.

Figure 18 shows the test results: the trend, summarised in Table 6, show the same behaviour as the benchmark circuit tests.

Configuration	Tolerated Attackers (0-6)
Raw circuit cutting	0
Proportional probability and 2X replication	1
Exponential probability and 2X replication	4
Exponential probability and 3X replication	3
Exponential probability without replication	5

Table 6. Summary of integrity-related experimental results on the GHZ circuit.

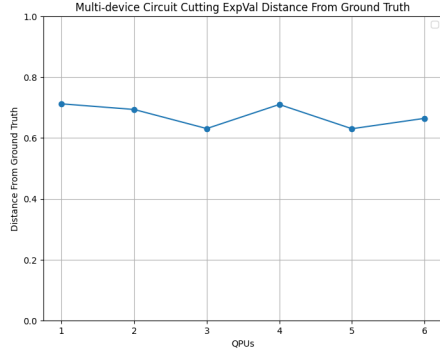
4.2.6 Further tests: Deutsch-Jozsa Algorithm Circuit. The Deutsch-Jozsa algorithm solves the following problem: given an oracle that implements a function $f : 0, 1^n \rightarrow 0, 1$, determine whether f is *constant*: if f is constant, it will return the same value – either 0 or 1 – no matter the input; if f is *balanced* it will return 0 for exactly half of the possible input and 1 for the other half.

The standard deterministic algorithm would require, in the worst case, at least $2^{(n-1)} + 1$ evaluations of f , where n is the number of bits. The quantum Deutsch-Jozsa algorithm, instead, provides the solution with a single evaluation of f .

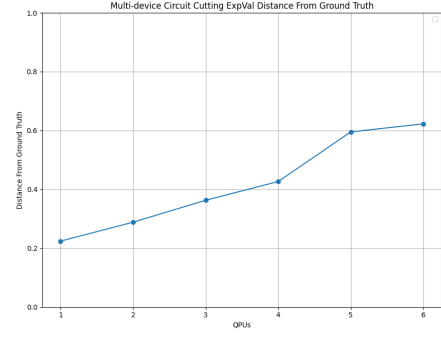
The quantum algorithm works as follows:

- (1) Define the initial state by using a n qubit register initialized to $|0\rangle$ and an auxiliary qubit initialized to $|1\rangle$:

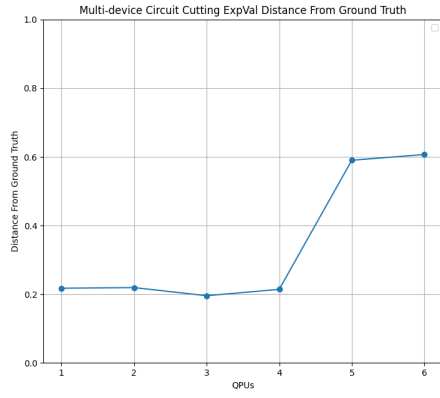
$$|0\rangle^{\otimes n} \otimes |1\rangle.$$



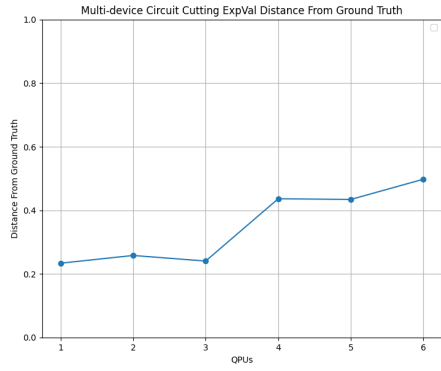
(a) Raw circuit cutting test results



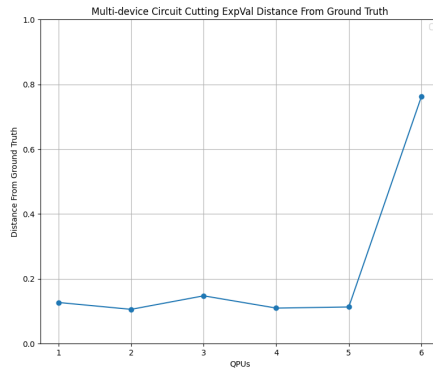
(b) Proportional probability and 2X replication test results



(c) Exponential probability and 2X replication test results



(d) Exponential probability and 3X replication test results



(e) Exponential probability without replication test results

Fig. 18. Integrity resilience tests on the GHZ circuit (Hellinger distance from ground truth with a growing number of attackers).

- (2) Apply a Hadamard gate H to each of the $n + 1$ qubits to create a quantum superposition in which all possible inputs are represented:

$$\frac{1}{\sqrt{2^n}} \sum_{x=0}^{2^n-1} |x\rangle \otimes \frac{|0\rangle - |1\rangle}{\sqrt{2}}.$$

- (3) Call the quantum oracle, implemented as a U_f port that acts on the qubits with the following transformation:

$$U_f : |x\rangle |y\rangle \rightarrow |x\rangle |y \oplus f(x)\rangle.$$

- (4) After the oracle call, the information about $f(x)$ is encoded in the input registry phase as follows:

$$\frac{1}{\sqrt{2^n}} \sum_{x=0}^{2^n-1} (-1)^{f(x)} |x\rangle \otimes \frac{|0\rangle - |1\rangle}{\sqrt{2}}.$$

- (5) Apply again the Hadamard gate to the first n qubits to transform the phases in amplitudes.
 (6) Measure the final state of the first n qubits: the resulting observation will always be $|0\rangle^{\otimes n}$ if the function is *constant*, otherwise it is *balanced*.

Figure 19 displays a Deutsch-Jozsa quantum circuit for a 3-bit function. It uses four qubits, including the auxiliary one.

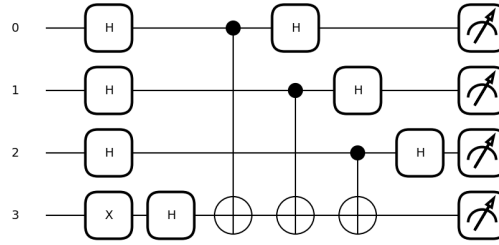


Fig. 19. Deutsch-Jozsa circuit for a 3 bit function.

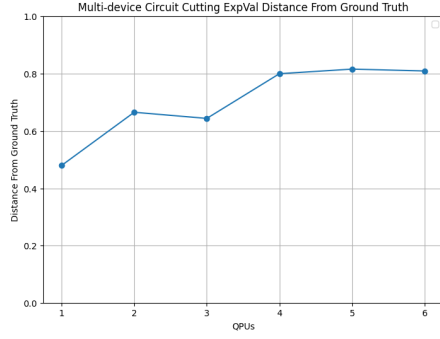
The same tests performed on the benchmark circuit and the GHZ circuit (see Subsection 4.2.5) have also been applied to a 15 qubit Deutsch-Jozsa circuit from the MQT benchmark suite [22] (with two circuit cuts applied):

- (1) raw circuit cutting;
- (2) proportional sub-circuit allocation probability and 2X replication;
- (3) exponential sub-circuit allocation probability and 2X replication;
- (4) exponential sub-circuit allocation probability and 3X replication;
- (5) exponential sub-circuit allocation probability without replication.

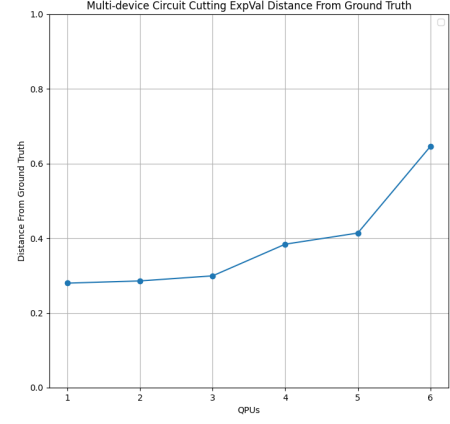
All tests have been executed with a growing number of attacking QPUs, from 1 to 6, and the corresponding distribution of expectation values was compared with the ground truth (the circuit executed without any offending QPU).

Figure 20 shows the test results: the trend, summarised in Table 7, is the same as that of the benchmark circuit tests.

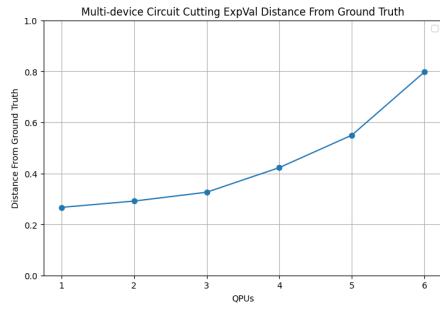
4.2.7 *Discussion of the Results.* Table 8 summarises the integrity-related experiments presented in this Section.



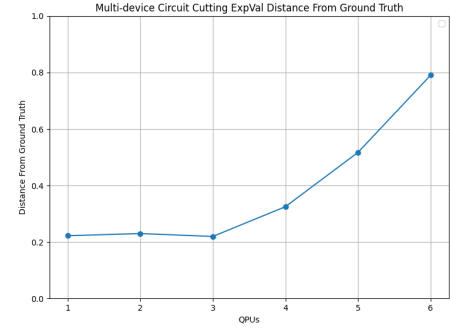
(a) Raw circuit cutting test results



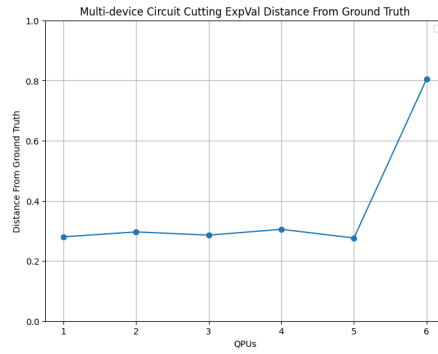
(b) Proportional probability and 2X replication test results



(c) Exponential probability and 2X replication test results



(d) Exponential probability and 3X replication test results



(e) Exponential probability without replication test results

Fig. 20. Integrity resilience tests on the Deutsch-Jozsa circuit (Hellinger distance from ground truth with a growing number of attackers)

Configuration	Tolerated Attackers (0-6)
Raw circuit cutting	0
Proportional probability and 2X replication	2
Exponential probability and 2X replication	2
Exponential probability and 3X replication	3
Exponential probability without replication	5

Table 7. Summary of integrity-related experimental results on the Deutsch-Jozsa circuit.

Configuration	Tolerated Attackers (0-6)		
	Benchmark	GHZ	Deutsch-Jozsa
Raw circuit cutting	0	0	0
Proportional probability and 2X replication	3	1	2
Exponential probability and 2X replication	4	4	2
Exponential probability and 3X replication	3	3	3
Exponential probability without replication	5	5	5

Table 8. Summary of integrity-related experimental results.

It is therefore evident that **Goal G1** (stated in Subsection 3.3), can be achieved through quantum circuit cutting, enhanced with sub-circuit allocation probabilities that are exponential with respect to dynamic integrity scores computed using suitable probe circuits.

4.2.8 Proportional VS Exponential Sub-Circuit Allocation Probability. Among the countermeasures described in Section 3.4, the sub-circuit QPU allocation probability emerges as the most critical factor in determining the optimal quantum circuit cutting configuration for integrity resilience.

The tests in Section 4.2 used two different functions to determine the probability P_n of selecting n^{th} QPU:

- **Proportional:** $\frac{IS_n}{\sum_{i=0}^5 IS_i}$
- **Exponential:** $\frac{e^{IS_n}}{\sum_{i=0}^5 e^{IS_i}}$

Both formulae take into account the QPUs *integrity scores* IS .

As discussed in subsection 4.2.7, the advantage of the exponential probability model is evident. To understand why, we examine the average QPU sub-circuit allocation percentages under an increasing number of saboteurs, from 0 to 6. Figure 21 shows the allocation percentages for the proportional model, while Figure 22 shows those for the exponential model. The percentages were computed by averaging the sub-circuit allocation rate of each experiment, grouped by allocation policy (proportional or exponential) and number of active saboteurs.

Clearly, the exponential probability formula is much more aggressive than the proportional one, as it tends to underutilize even good-behaving QPUs when their integrity score is just slightly lower than the best-performing ones. However, QPUs with a very low score, and therefore defective or malicious, are guaranteed to have little to no sub-circuits assigned up to 5 attacking devices over 6. While the proportional probability formula ensures a more balanced allocation across all devices, it also results in poorly performing QPUs consistently receiving a significant share of sub-circuits.

Overall, the rationale behind the choice of these models can be understood as a trade-off between integrity resilience (a cybersecurity preference) and load distribution (a performance and possibly cost preference). To fulfil **Goal G1** (ensuring integrity resilience), the exponential probability model appears to be the most effective choice; however, this may not always hold true in different contexts.

4.3 Confidentiality Testing

To fulfill **Goal G2** (see section 3.3), our experiments aim to verify whether circuit cutting (possibly enhanced with additional countermeasures) can ensure the confidentiality of the input circuit. Intuitively, circuit cutting alone can help invalidate parts of the circuit and output data from being exposed to untrusted QPUs, simply by avoiding the allocation of all sub-circuits to a single QPU.

However, our PNI-inspired testing methodology requirement is more stringent: ideally, the QPUs should not be able to distinguish between different inputs. In other words, they should not be able to pinpoint the actual computation that they have been tasked to perform. The experimental results summarised in this section, therefore, aim to measure the capability of malicious QPUs to distinguish between different input circuits.

Note that the output data being analysed will be the complete set of individual QPUs output values, possibly including fake circuit outputs, without reconstructing them through the post-processing algorithm. To understand the rationale behind it, we shall revisit the PNI definition of confidentiality:

$$P(O_{lo}|I_{hi}) \simeq P(O_{lo}|I_{hi'}), \quad (9)$$

where:

- I_{hi} and $I_{hi'}$ are two high-level inputs fully available to the scheduler that malicious QPUs are trying to distinguish;
- O_{lo} is the low-level output produced by each QPU.

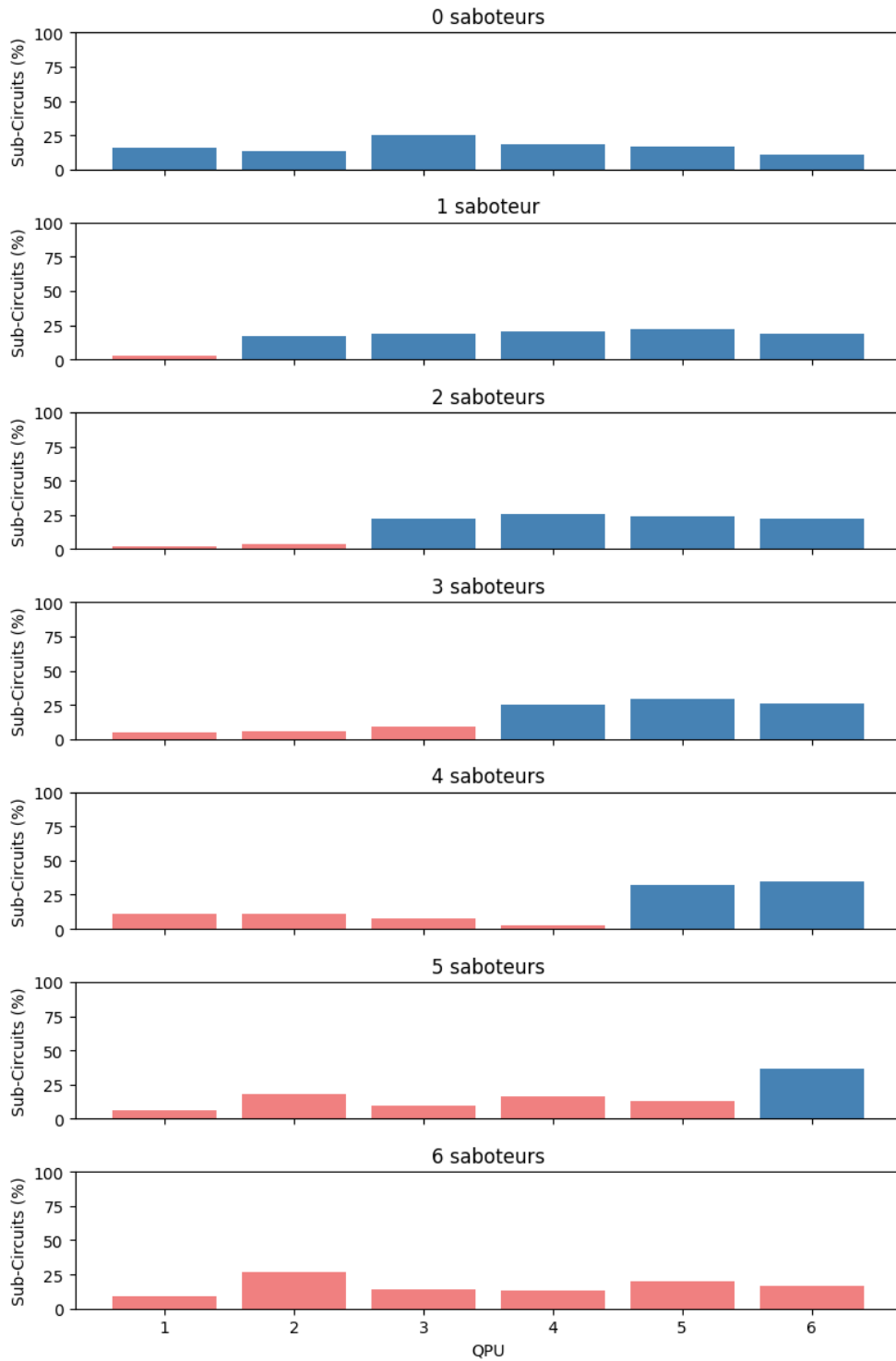
The high-level output O_{hi} obtained by combining the low-level outputs of the QPUs, is not involved in the confidentiality testing.

Verifying whether Equation 9 holds is non-trivial for several reasons:

With a raw circuit cutting scheme, different high-level inputs I_{hi} give rise to different sub-circuits, which in turn produce different low-level outputs O_{lo} . One possible way to mitigate this issue is to flood the QPUs with fake sub-circuits, thereby diluting the actual results (see the corresponding additional countermeasure defined in Section 3.4). However, demonstrating the effectiveness of this dummy sub-circuit flooding technique using histograms and Hellinger distances from the ground truth is challenging. The fake values would need to fall within the expected range and approximate magnitude of legitimate outputs; otherwise, they risk being discarded or simply ignored. Note that, in the general case, it is not possible to know the correct output of the original quantum circuit evaluation prior to execution, which complicates the design of effective strategies.

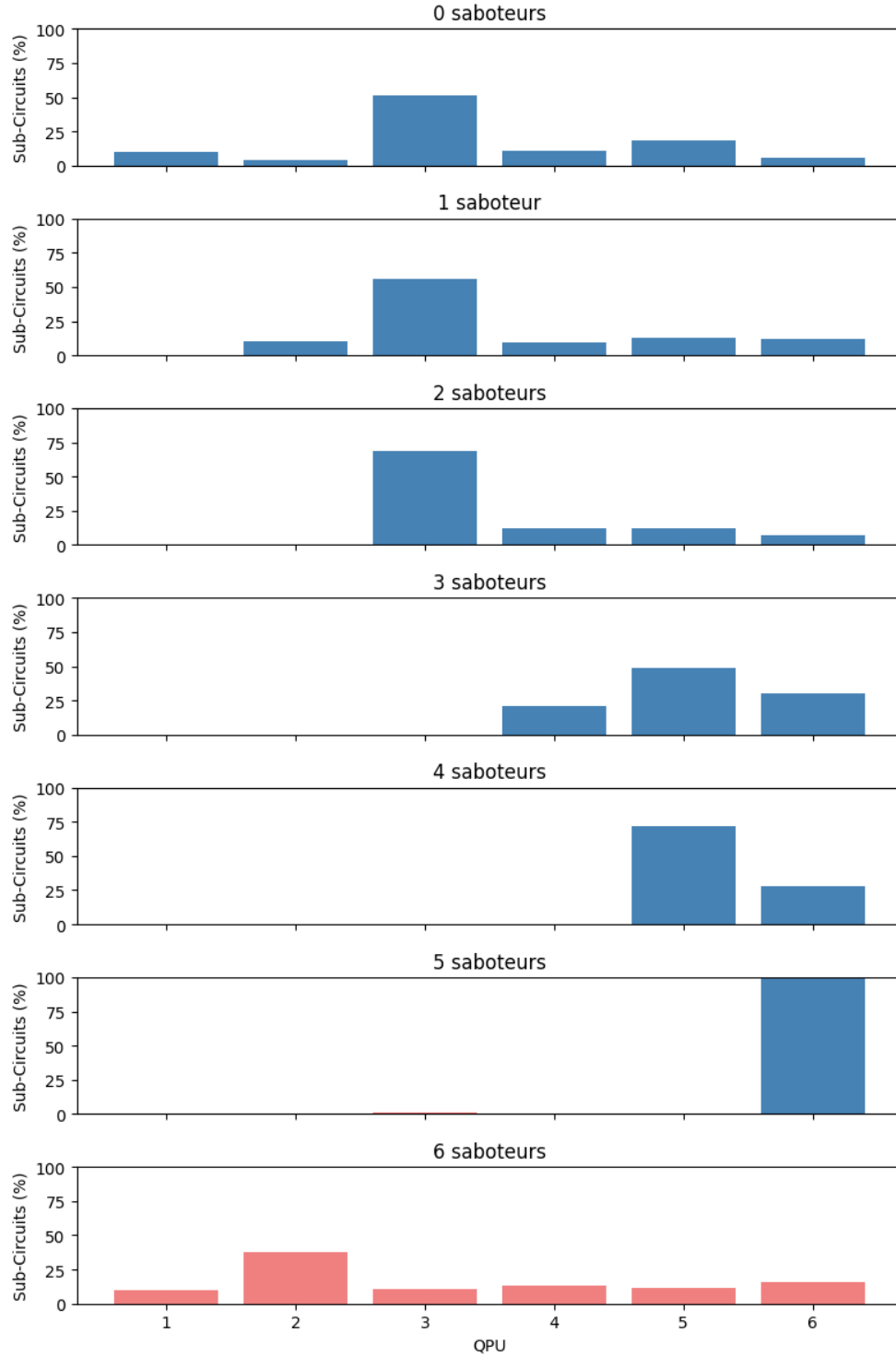
Our testing procedure, therefore, is structured as follows:

- (1) verifying that two different input circuits I_{hi} and $I_{hi'}$ result in different low-level output distributions O_{lo} and $O_{lo'}$;
- (2) verifying the impact of genuinely random fake circuits in the low-level output distribution O_{lo} ;
- (3) verifying the impact of artificially constructed fake circuits whose results are within the same magnitude as the real one.



Manuscript submitted to ACM

Fig. 21. Proportional sub-circuit allocation probability with a growing number of saboteurs. The percentages have been computed by averaging the sub-circuit allocation rate of each experiment with proportional sub-circuit allocation probability, grouped by the number of active saboteurs.



Manuscript submitted to ACM

Fig. 22. Exponential sub-circuit allocation probability with a growing number of saboteurs. The percentages have been computed by averaging the sub-circuit allocation rate of each experiment with exponential sub-circuit allocation probability, grouped by the number of active saboteurs.

The number of fake circuits used in the tests will be determined by a multiplier m : for each legitimate sub-circuit, each QPU will also have to process m fake circuits.

In the confidentiality testing, attackers play a passive role and are typically undetectable. The scheduler user can provide *confidentiality scores* based on information about the QPUs and their operators (see Section 3.4). However, in the following tests, we will assume that all the processors have equal confidentiality score.

4.3.1 First Test: Raw Circuit Cutting. It is not surprising that raw circuit cutting might provide the user with a certain degree of confidentiality, given that individual QPUs receive only fragments of the original quantum circuit. However, the requirement that each QPU be unable to distinguish between different high-level input circuits is, intuitively, not satisfied, as different input circuits inevitably result in different sub-circuits and, consequently, different output values.

The numerical comparison of the Hellinger distances between the low-level QPUs outputs of the benchmark circuits confirms this hypothesis. Table 9 and Figure 23 illustrate such distances, which are very close to the upper limit, meaning that a malicious QPU can easily distinguish between different input circuits. Note that the PNI-inspired constraint defined in Section 3 is not satisfied.

Comparison Circuit	Hellinger Distance
Alternative benchmark	0.991
GHZ	0.923
Deutsch-Jozsa	0.837

Table 9. Low-level output Hellinger distance from reference benchmark circuit with raw circuit cutting

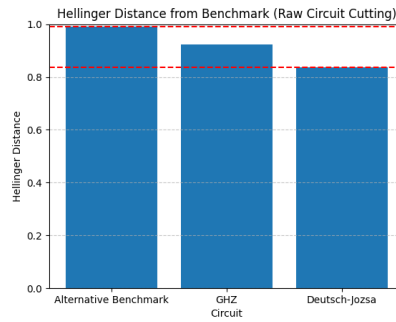


Fig. 23. Hellinger distance from benchmark circuit low-level QPU output data with raw circuit cutting (lower is better, the red dotted lines delimit visually the range between the maximum and minimum value).

4.3.2 Second Test: 5X Fake Circuits. Using five fake circuits for each real sub-circuit reduces the overall Hellinger distance between the QPUs low-level outputs in the presence of different input circuits. However, as it can be seen in Tables 10, 11, and in Figure 24, genuinely random fake circuits do not introduce anywhere near as much noise as calibrated ones.

Comparison Circuit	Hellinger Distance (random)
Alternative benchmark	0.880
GHZ	0.891
Deutsch-Jozsa	0.898

Table 10. Low-level output Hellinger distance from reference benchmark circuit with 5X random fake circuits.

Comparison Circuit	Hellinger Distance (calibrated)
Alternative benchmark	0.163
GHZ	0.206
Deutsch-Jozsa	0.328

Table 11. Low-level output Hellinger distance from reference benchmark circuit with 5X calibrated fake circuits.

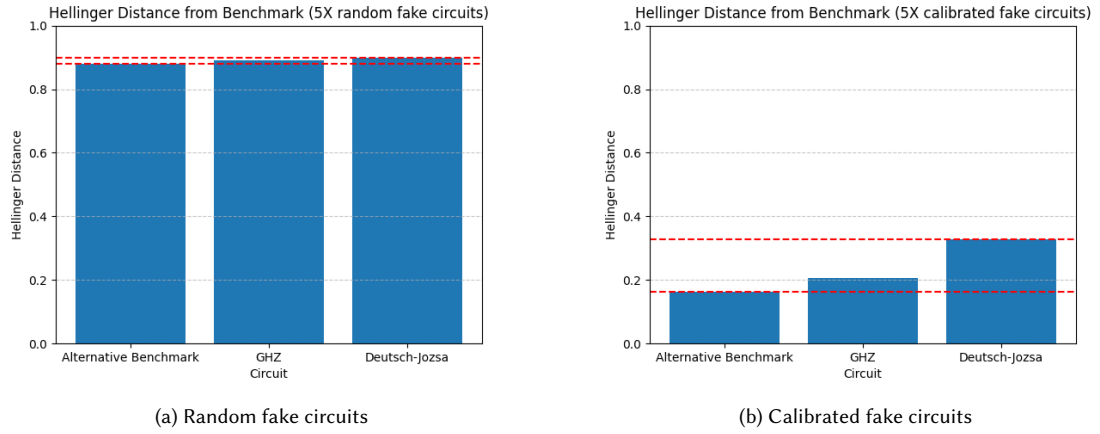


Fig. 24. Hellinger distance from benchmark circuit low-level QPU output data with 5X fake circuits (lower is better, the red dotted lines delimit visually the range between the maximum and minimum value).

4.3.3 Third Test: 10X Fake Circuits. In the final confidentiality-related test, for each sub-circuit, 10 fake circuits were also sent to each QPU. The results, displayed in Tables 12 and 13, and in Figure 25, are even better than the ones with the 5X multiplier. As in the previous experiments, calibrated fake circuits remain the only option that provides sufficient noise to effectively mask differences between input circuits.

Comparison Circuit	Hellinger Distance (random)
Alternative benchmark	0.826
GHZ	0.753
Deutsch-Jozsa	0.742

Table 12. Low-level output Hellinger distance from reference benchmark circuit with 10X random fake circuits

4.3.4 Discussion of the Results. Figure 26 summarises the overall performance of truly random and calibrated fake circuits over different algorithms. With respect to the PNI-inspired constraint defined in Section 3, which measures

Comparison Circuit	Hellinger Distance (calibrated)
Alternative benchmark	0.107
GHZ	0.172
Deutsch-Jozsa	0.157

Table 13. Low-level output Hellinger distance from reference benchmark circuit with 10X calibrated fake circuits

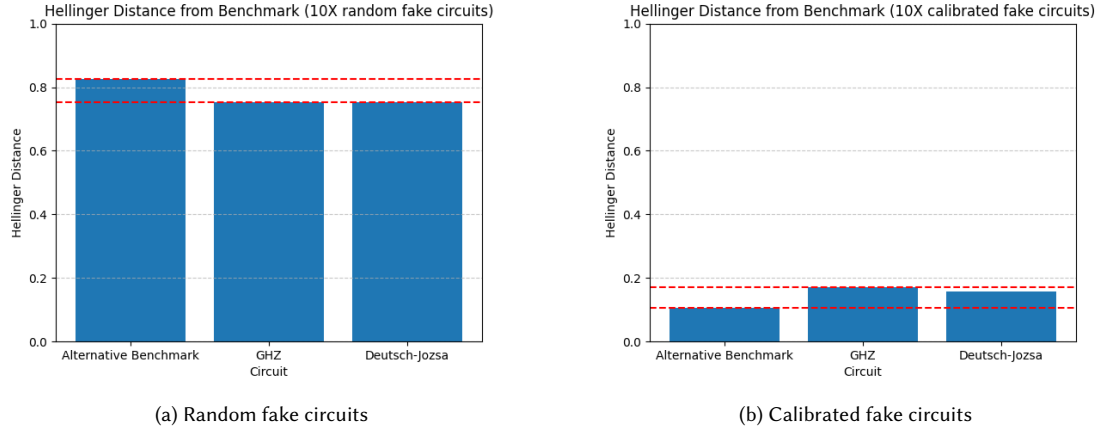


Fig. 25. Hellinger distance from benchmark circuit low-level QPU output data with 10X fake circuits (lower is better, the red dotted lines delimit visually the range between the maximum and minimum value).

each QPU's ability to distinguish between different inputs. Note that the use of calibrated fake circuits yields superior performance compared to random fake circuits, given the same multiplier.

Wherever possible, calibrated sub-circuits should be the preferred countermeasure for obfuscating high-level, sensitive input from malicious QPUs. In the general case, however, when it is not possible to estimate the magnitude and the range of a quantum circuit, truly random fake circuits can still offer a degree of confidentiality protection, even though they need higher multipliers with respect to calibrated ones. Additionally, it is important to note that circuit cutting inherently offers a level of input hiding by design, as long as no single QPU receives the entire set of sub-circuits (see Subsection 4.3.5 for further discussion).

Overall, fulfilling **Goal G2**, as defined in Subsection 3.3, is possible through the use of fake circuits in conjunction with circuit cutting, supported by the security countermeasures outlined in Subsection 3.4.

4.3.5 Proportional VS Exponential Sub-Circuit Allocation Probability, Revisited. Subsection 4.3.5, in the context of integrity-related security, summarised how a sub-circuit allocation probability model (which is exponential with respect to each QPU's integrity score) produced the best results. However, this came at the cost of underutilising legitimate QPUs whose scores were only slightly lower than those of the best-performing ones, since saboteurs with very low scores were effectively ignored.

Note that, if we take into account the confidentiality of the input, allocating most of the work to a few or even a single QPU poses significant security concerns. While the integrity-related attack surface is reduced, the confidentiality-related

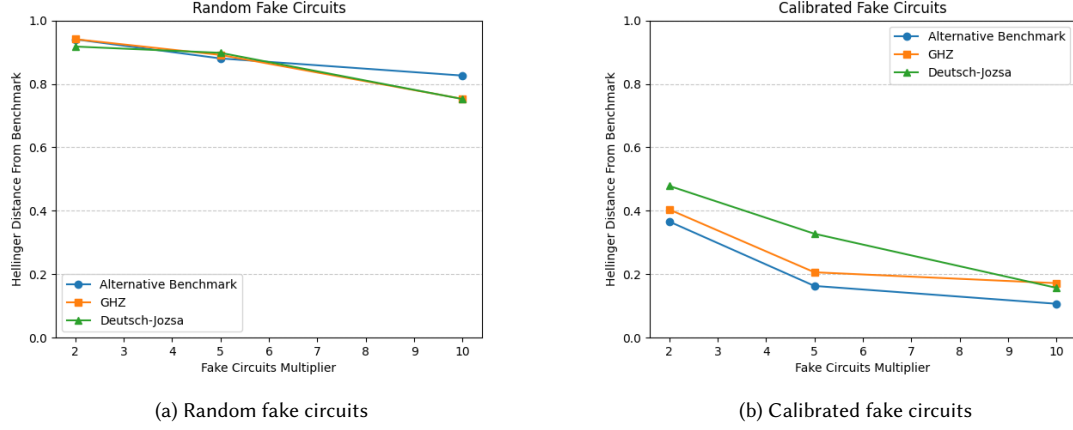


Fig. 26. Hellinger distance from benchmark circuit low-level QPU output data with fake circuits (lower is better).

attack surface is extended. The proportional probability model guarantees a better input data distribution, which is obviously safer from a secrecy point of view.

Therefore, the proportional probability model for allocating sub-circuits to the QPUs is the most convenient choice if input data (the quantum circuit, which may represent valuable IP) confidentiality, is the asset to protect. In contrast, exponential probability is still the best choice when output data correctness is deemed more important.

4.4 Experimental Methodology Generalization

The tests carried out to verify the resilience of various quantum circuit cutting schemes against integrity and confidentiality attacks represent not only a detailed validation of the proposed techniques, but it is also an example of the application of an experimental methodology guided by the principles of PNI. This approach provides a conceptual framework that allows us to transform scenarios into quantitative metrics that, due to the nature of quantum computing and the specifics of security threats, are otherwise considerably difficult to evaluate objectively.

The adoption of a probabilistic framework such as PNI allows the translation of security requirements (e.g., "an attacker must not influence the global output" or "a processor must not distinguish between two different inputs") into experimentally verifiable statistical relationships.

This approach is independent of the type of security technique under consideration and can therefore be reused to evaluate other protection strategies in distributed quantum systems. In other words, the methodology applied here for quantum circuit cutting constitutes a general model that can guide the design of experimental security property validations, providing a common framework for comparing different approaches and guiding system designer decisions.

5 RELATED WORK

The research in the field of quantum-cloud security techniques is considerably dynamic. In this section we outline the state of the art with respect to techniques for the protection of integrity and confidentiality of quantum computations, and to verify their effectiveness.

5.1 Integrity Protection

Noise measurement and noise injection techniques, exploiting the physical error processes that naturally arise in current NISQ devices. By deliberately adding calibrated crosstalk or depolarising noise, these methods embed a fragile “watermark” in the computation: any adversarial perturbation that exceeds the calibrated envelope can be statistically detected. Recent works [16] shows that controlled crosstalk can improve the resistance of quantum-mapped deep neural networks against gradient-based attacks, increasing robustness on MNIST, CIFAR-10, and CIFAR-100 benchmarks by up to 268%. However, the approach remains limited to circuits whose logical structure tolerates additional noise.

5.2 Confidentiality Protection

Quantum circuit obfuscation is a family of confidentiality-preserving techniques that seek to conceal structural information gate types, data flow, and algorithmic intent, while preserving functional correctness. Two main families of obfuscation techniques dominate the literature:

- (1) **Dummy-gate insertion:** strategically placed reversible gates (often CNOT) amplify the total variation distance (TVD) between the obfuscated and original output distributions, while barriers allow legitimate users to strip dummy entities after the circuit compilation [27].
- (2) **Circuit embedding:** random reversible sub-circuits are interleaved with the target circuit, increasing the search space that an attacker must traverse [11].

Both strategies increase the computation confidentiality, but they can conflict with compiler optimisations. Moreover, retaining obfuscation metadata without exposing it to a malicious toolchain remains an open engineering challenge.

A second notable family of techniques for confidentiality protection is Blind quantum computation (BQC). BQC protocols guarantee information-theoretic privacy by allowing a client to delegate quantum computation to an untrusted server without revealing information on input, algorithm, or output. The archetypal protocol by Broadbent [9] and its later refinements rely on the client ability to prepare single-qubit states $|t_\theta\rangle$ with hidden phases and to engage in interactive, measurement-based classical communication. While BQC may provide strong privacy and verifiability (via trap qubits), it assumes minimal quantum capabilities on the client side and incurs in substantial latency from round-trip interactions. These requirements are incompatible with purely classical clients.

Finally, an interesting set of confidentiality-preserving techniques are Quantum homomorphic encryption (QHE) schemes. QHE extends the classical notion of computation on encrypted data to the quantum domain. Tan [28] introduced a private-key bosonic scheme in which encryption acts on internal degrees of freedom while computation acts on spatial modes, bounding the Holevo information by $\chi \leq m \log_2 m$. Follow-up photonic prototypes demonstrated the principle experimentally but they remain limited to small-dimensional Hilbert spaces and non-interactive gate sets. Fundamental obstacles currently restrict QHE to proof-of-concept demonstrations: the no-cloning theorem, decoherence under ciphertext growth, and polynomial overheads for universal gate sets.

5.3 Noninterference-based Quantum Circuit Security Validation

Recently, Ying et al. proposed an extension of the classical PNI model for the formal verification of the security properties of quantum algorithms [30]. In the quantum context, the presence of entanglement and the inevitable state alteration due to measurements introduce new challenges, making classical PNI formulations indirectly inapplicable. To address these peculiarities, a quantum automaton model has been proposed that uses density operators, superoperators, and POVM measurements to describe the evolution of the system and observations of the agents. On this basis, noninterference is

reformulated in terms of the insecurity degree, which quantifies the extent of possible interference between groups of agents, and an approximate version is introduced to account for noise and physical imperfections. The approach is supported by a generalisation of the unwinding technique for formal verification, which allows for the estimation of upper bounds on the insecurity degree, and by a compositionality theorem that ensures the preservation of security in composite systems, in the absence of entanglement between components.

5.4 Positioning of This Work

Existing integrity checks, such as noise injection, are algorithm-specific; circuit obfuscation alone does not ensure correctness; BQC mandates a quantum-capable client, and QHE is still impractical for medium-scale circuits.

Our paper addresses these gaps by proposing a generic circuit cutting-based approach that can be easily implemented and integrated in existing quantum-cloud infrastructures. Unlike prior art, our method scales to any number of logical qubits without client-side quantum resources, bridging the gap between near-term NISQ capabilities and cryptographic-grade security requirements both in terms of information integrity and confidentiality.

6 CONCLUSIONS

In this paper, we discussed whether quantum circuit cutting (when properly enhanced) can serve not only as a circuit decomposition technique to make use of QPUs with a limited number of qubits, but also as an effective security mechanism. In particular, we aimed to explore and outline a set of security countermeasures that, when combined with circuit cutting, can enhance the integrity and confidentiality of quantum computations in potentially untrusted or adversarial environments.

As outlined in Subsection 3.3, the objectives of this work are as follows:

- Goal G1:** Proposing a methodology to improve the *integrity* of output data while using potentially untrusted quantum processors through a trusted centralised scheduler.
- Goal G2:** Proposing a methodology to improve the *confidentiality* of algorithms and input/output data while using potentially untrusted quantum processors through a trusted centralised scheduler.
- Goal G3:** Designing a methodological framework for quantum computational system designers to compare different quantum architectures with respect to integrity and confidentiality resilience.

To address both goals, **G1** and **G2**, the key idea was to use enhanced quantum circuit cutting. In light of the experimental results presented in Section 4, we now revisit the contributions of this work with respect to the previously stated goals.

6.0.1 Goal G1. The resilience of quantum circuit cutting with respect to integrity has been analyzed within the guidelines of the Probabilistic Noninterference (PNI) framework under several configurations:

- (1) raw quantum circuit cutting;
- (2) circuit cutting enhanced with dynamic QPU integrity scores, sub-circuit distribution with a probability proportional to such scores, and a 2X sub-circuit replication factor with weighted averaging of QPU results;
- (3) same as above, but with a probability exponential with respect to integrity scores and a 2X sub-circuit replication;
- (4) same as above, but with a 3X sub-circuit replication;
- (5) same as above, but without sub-circuit replication.

The last configuration is the one that yields the best results:

- dynamic integrity scores computed with probe circuits evaluation by each QPU;
- sub-circuit allocation probabilities for each QPU exponential with respect to integrity scores;
- no sub-circuit replication.

This configuration yields the best results even with 5 attacking QPUs over 6. The technique can be easily implemented and integrated within existing shot-wise quantum broker architectures such as [6] and [8].

6.0.2 Goal G2. The PNI-inspired requirement for confidentiality is that the QPUs should not be able to distinguish between different input circuits. Raw circuit cutting, while offering a degree of secrecy for both input and output data by dividing the quantum circuit into multiple sub-circuits allocated to different QPUs, falls short of meeting this more stringent requirement.

Fake circuits were mixed with real sub-circuits obtained by quantum circuit cutting to hide input circuit differences to the QPUs. Calibrated fake circuits¹ with a specific multiplier (e.g., five fake circuits for each real sub-circuit) yielded the best results. With a 5X or greater multiplier, input circuit differences are effectively hidden to the individual QPUs. In the general case, where no information is available about the characteristics of the input circuit's expectation values, random fake sub-circuits can still be used. However, it should be noted that they require a larger multiplier than calibrated fake circuits to achieve a comparable level of confidentiality protection.

We tested several multipliers (2X, 5X, and 10X) with different algorithms (custom benchmark circuits, GHZ and Deutsch-Jozsa), and the overall trend is that higher fake circuit multipliers provide greater input data obfuscation. The optimal choice of multiplier depends on the trade-off between the relevance assigned to input data confidentiality and the cost associated with processing fake data.

Overall, quantum circuit cutting enhanced with fake circuit flooding (calibrated fake circuits, when possible) provides an adequate confidentiality protection for the input data of quantum computations. Note that these countermeasures can also be easily integrated into existing shot-wise quantum broker architectures such as [6] and [8].

6.0.3 Goal G3. The PNI-inspired heuristics have proven themselves effective in terms of system design explorations:

- (1) Estimating the integrity resilience of a specific architecture can be performed by means of QPU simulators, whose outputs will be stored firstly unaltered, then corrupted by an increasing number of malicious Quantum Processing Units (QPUs). The attacker capabilities can be defined flexibly, depending on the context, and the results are obtained in a relatively short amount of time.
- (2) Estimating confidentiality resilience requires some care with respect to the input provided to the system: truly random inputs will hardly satisfy the PNI-inspired constraints. Therefore, calibrated inputs that produce outputs close to the ground truth are the preferable option.

The heuristics defined in this paper can be readily integrated into quantum software engineering workflows, as they require relatively little time to execute and provide system designers with valuable guidance on specific security properties. However, as shown in Subsection 4.3.5, a rigorous assessment of trade-offs is still needed, since different security properties may lead to conflicting requirements. It is therefore the responsibility of the system designer to reconcile these conflicts while keeping the overall system objectives in mind. This reflects a broader principle in software engineering: even in the case of quantum computing, security must be treated as a first-class design concern, carefully balanced against performance, usability, and other non-functional requirements throughout the development lifecycle.

¹Fake circuits whose expectation values fall within the range of the actual sub-circuits expectation values and are of a comparable magnitude.

6.1 Secure Quantum Scheduler

An notable application of the security techniques proposed in this work is the design of a secure scheduler within the cloud-based quantum computing scenario outlined in Subsection 3.1. Here, we reflect on this issue and discuss its implications for system architecture and trust assumptions.

The secure scheduler should protect the user’s quantum circuit (the input) and its computation results (the output), respectively, from a confidentiality and integrity point of view. As stated in Subsection 4.3.5, there are trade-offs to be made depending on whether input data confidentiality or output data integrity are deemed more important. In real-world contexts, users often operate under different constraints, and a secure system should enable them to make the best choices based on their specific needs.

To simplify the end user’s decision-making, the secure scheduler can offer three macro-configurations based on the user’s security preferences. Each configuration combines quantum circuit cutting with the additional countermeasures defined in Subsection 3.4². A hypothetical scheduler user could specify the desired security profile along with other computation-related parameters through a user interface or a manifest file, possibly fine-tuning specific parameters if needed. Note that the following configurations are only meant to show the interplay between the findings related to **Goal G1** (integrity) and **Goal G2** (confidentiality); the specific set of security countermeasures and their parameters will have to undergo experimental verification before being usable in security-critical contexts.

The three configurations presented below represent different balance points between two often competing objectives: protecting input confidentiality and protecting output integrity. The choice of a specific profile depends on the operational context and the type of risk perceived by the user.

Configuration 1 - Confidentiality Over Integrity:

- Fake sub-circuits with a 10X factor compared to the real ones (the user can optionally fine-tune the factor).
- Integrity probe circuits to compute integrity scores.
- Sub-circuit allocation probabilities *proportional* to the sum of the confidentiality score CS multiplied by two and the QPUs dynamic integrity score IS :

$$\frac{2CS_n + IS_n}{\sum_{i=1}^{n_qpus} 2CS_i + IS_i}, \quad (10)$$

where n is the current QPU index and n_qpus is the number of available QPUs.

This configuration prioritises confidentiality, assuming scenarios where unauthorised access to the quantum circuit is the primary threat (e.g., multi-tenant environments where untrusted operators manage the processors). Using a high factor of fake circuits reduces the ability of malicious QPUs to distinguish the real circuit.

Configuration 2 - Balanced:

- Fake sub-circuits with a 5X factor compared to the real ones (the user can optionally fine-tune the factor).
- Integrity probe circuits to compute integrity scores.
- Sub-circuit allocation probabilities *proportional* to the sum of the QPUs dynamic integrity score IS and the confidentiality score CS :

$$\frac{CS_n + IS_n}{\sum_{i=1}^{n_qpus} CS_i + IS_i}, \quad (11)$$

²Please note that sub-circuit replication is not included, since the experiments of subsection 4.2 proved it to be detrimental to integrity resilience and, intuitively, distributing the same sub-circuit to more than one QPU broadens the confidentiality attack surface as well.

where n is the current QPU index and n_qpus is the number of available QPUs.

This configuration is designed for scenarios where both confidentiality and integrity are important and the risk is distributed. The false circuit factor and the equal weighting between confidentiality and integrity scores aim to provide balanced protection, reducing overall risk without optimising one objective at the expense of the other. It is suitable for contexts where it is not possible to determine a priori which threat is predominant.

Configuration 3 - Integrity over Confidentiality:

- Fake sub-circuits with a 2X factor compared to the real ones (the user can optionally fine-tune the factor).
- Integrity probe circuits to compute integrity scores.
- Sub-circuit allocation probabilities *exponential* with respect to the sum of QPUs dynamic integrity score IS multiplied by two and the confidentiality score CS :

$$\frac{e^{2IS_n + CS_n}}{\sum_{i=0}^{n_qpus} e^{2IS_i + CS_i}}, \quad (12)$$

where n is the current QPU index and n_qpus is the number of available QPUs.

This configuration is suitable when the accuracy of the final result is a priority, such as critical applications where altered output could cause serious consequences. The reduced number of falsified circuits limits the overhead and maintains a high quality of the data used for output reconstruction. Allocation probabilities strongly favour QPUs with high integrity scores, making it more difficult for an attacker to significantly alter the overall result.

6.2 Future Work

To conclude, we outline several promising research directions that could further develop the use of quantum circuit cutting as a security technique for enhancing integrity and confidentiality.

Delayed integrity probes: rather than sending integrity probes upfront, before the actual quantum computation, they could be mixed at any later point of sub-circuit execution, be it the middle or even the end; by doing this, especially in combination with fake circuits, it would become more challenging for malicious QPUs to detect and avoid the probes, making the integrity score more reliable.

Improved integrity probes: noise injection and measurement techniques could be used instead of or together with circuits with known expectation values;

Sub-circuits as integrity probes: replicated sub-circuit evaluation could be used as an integrity probe if most of the QPUs are considered reliable.

Integration with alternative security techniques: security techniques such as Circuit Obfuscation (see Section 5) could be integrated with quantum circuit cutting as further security enhancements and evaluated through the PNI-based methodology used in this work.

Secure Quantum Scheduler: explore the integration of integrity and confidentiality-related security countermeasures in a real-world context to provide end-users with a robust and usable system (Subsection 6.1 sketches a hypothetical direction for this line of research).

REFERENCES

- [1] Alán Aspuru-Guzik, Anthony D Dutoi, Peter J Love, and Martin Head-Gordon. 2005. Simulated quantum computation of molecular energies. *Science* 309, 5741 (2005), 1704–1707.

- [2] Michael Backes and Birgit Pfizmann. 2004. Computational probabilistic noninterference. *International Journal of Information Security* 3, 1 (2004), 42–60.
- [3] Aleksandrs Belovs. 2019. Quantum algorithms for classical probability distributions. *arXiv preprint arXiv:1904.02192* (2019).
- [4] Ville Bergholm, Josh Izaac, Maria Schuld, Christian Gogolin, Shah Nawaz Ahmed, Vishnu Ajith, M Sohaib Alam, Guillermo Alonso-Linaje, B Akash-Narayanan, Ali Asadi, et al. 2018. PennyLane: Automatic differentiation of hybrid quantum-classical computations. *arXiv preprint arXiv:1811.04968* (2018).
- [5] Giuseppe Bisicchia, Alessandro Bocci, José García-Alonso, Juan M Murillo, and Antonio Brogi. 2024. Cut&Shoot: Cutting & Distributing Quantum Circuits Across Multiple NISQ Computers. In *2024 IEEE International Conference on Quantum Computing and Engineering (QCE)*, Vol. 2. IEEE, 187–192.
- [6] Giuseppe Bisicchia, Jose García-Alonso, Juan M. Murillo, and Antonio Brogi. 2023. Distributing Quantum Computations, by Shots. In *Service-Oriented Computing*, Flavio Monti, Stefanie Rinderle-Ma, Antonio Ruiz Cortés, Zibin Zheng, and Massimo Mecella (Eds.). Springer Nature Switzerland, Cham, 363–377.
- [7] Giuseppe Bisicchia, Jose García-Alonso, Juan M Murillo, and Antonio Brogi. 2024. From Quantum Software Handcrafting to Quantum Software Engineering. In *2024 IEEE International Conference on Software Analysis, Evolution and Reengineering-Companion (SANER-C)*. IEEE, 149–150.
- [8] Giuseppe Bisicchia, José García-Alonso, Juan M. Murillo, and Antonio Brogi. 2023. Dispatching Shots Among Multiple Quantum Computers: An Architectural Proposal. In *2023 IEEE International Conference on Quantum Computing and Engineering (QCE)*, Vol. 02. 195–198. doi:10.1109/QCE57702.2023.10210
- [9] Anne Broadbent, Joseph Fitzsimons, and Elham Kashefi. 2009. Universal blind quantum computation. In *2009 50th annual IEEE symposium on foundations of computer science*. IEEE, 517–526.
- [10] Daniel T Chen, Ethan H Hansen, Xinpeng Li, Vinooth Kulkarni, Vipin Chaudhary, Bin Ren, Qiang Guan, Sanmukh Kuppannagari, Ji Liu, and Shuai Xu. 2023. Efficient quantum circuit cutting by neglecting basis elements. In *2023 IEEE International Parallel and Distributed Processing Symposium Workshops (IPDPSW)*. IEEE, 517–523.
- [11] Subrata Das and Swaroop Ghosh. 2023. Randomized reversible gate-based obfuscation for secured compilation of quantum circuit. *arXiv preprint arXiv:2305.01133* (2023).
- [12] Samudra Dasgupta and Travis S Humble. 2021. Stability of noisy quantum computing devices. *arXiv preprint arXiv:2105.09472* (2021).
- [13] Daniel M. Greenberger, Michael A. Horne, and Anton Zeilinger. 2007. Going Beyond Bell’s Theorem. arXiv:0712.0921 [quant-ph] <https://arxiv.org/abs/0712.0921>
- [14] Ali Javadi-Abhari, Matthew Treinish, Kevin Krsulich, Christopher J. Wood, Jake Lishman, Julien Gacon, Simon Martiel, Paul D. Nation, Lev S. Bishop, Andrew W. Cross, Blake R. Johnson, and Jay M. Gambetta. 2024. Quantum computing with Qiskit. doi:10.48550/arXiv.2405.08810 arXiv:2405.08810 [quant-ph]
- [15] Mustafa Kaiiali, Sakir Sezer, and Ayesha Khalid. 2019. Cloud computing in the quantum era. In *2019 IEEE conference on communications and network security (CNS)*. IEEE, 1–4.
- [16] Shamik Kundu, Navnil Choudhury, Sanjay Das, Arnab Raha, and Kanad Basu. 2024. QNAD: Quantum Noise Injection for Adversarial Defense in Deep Neural Networks. In *2024 IEEE International Symposium on Hardware Oriented Security and Trust (HOST)*. IEEE, 1–11.
- [17] Shunlong Luo and Qiang Zhang. 2004. Informational distance on quantum-state space. *Physical Review A—Atomic, Molecular, and Optical Physics* 69, 3 (2004), 032106.
- [18] Juan M. Murillo, Jose Garcia-Alonso, Enrique Moguel, Johanna Barzen, Frank Leymann, Shaikat Ali, Tao Yue, Paolo Arcaini, Ricardo Pérez Castillo, Ignacio García Rodríguez de Guzmán, Mario Piattini, Antonio Ruiz-Cortés, Antonio Brogi, Jianjun Zhao, Andriy Miransky, and Manuel Wimmer. 2024. Quantum Software Engineering: Roadmap and Challenges Ahead. arXiv:2404.06825 [cs.SE] <https://arxiv.org/abs/2404.06825>
- [19] Tianyi Peng, Aram W Harrow, Maris Ozols, and Xiaodi Wu. 2020. Simulating large quantum circuits on a small quantum computer. *Physical review letters* 125, 15 (2020), 150504.
- [20] József Pitrik and Dániel Virosztek. 2020. Quantum Hellinger distances revisited. *Letters in Mathematical Physics* 110, 8 (2020), 2039–2052.
- [21] John Preskill. 2018. Quantum Computing in the NISQ era and beyond. *Quantum* 2 (Aug. 2018), 79. doi:10.22331/q-2018-08-06-79
- [22] Nils Quetschlich, Lukas Burgholzer, and Robert Wille. 2023. MQT Bench: Benchmarking Software and Design Automation Tools for Quantum Computing. *Quantum* (2023). MQT Bench is available at <https://www.cda.cit.tum.de/mqtbench/>.
- [23] Mijanur Rahaman and Md Masudul Islam. 2015. A review on progress and problems of quantum computing as a service (QaaS) in the perspective of cloud computing. *Global Journal of Computer Science and Technology* 15, 4 (2015).
- [24] Xiangyu Ren, Mengyu Zhang, and Antonio Barbalace. 2024. A Hardware-Aware Gate Cutting Framework for Practical Quantum Circuit Knitting. *arXiv preprint arXiv:2409.03870* (2024).
- [25] Manuel S. Rudolph, Jacob Miller, Danial Motlagh, Jing Chen, Atithi Acharya, and Alejandro Perdomo-Ortiz. 2023. Synergistic pretraining of parametrized quantum circuits via tensor networks. *Nature Communications* 14, 1 (Dec. 2023). doi:10.1038/s41467-023-43908-6
- [26] Peter W Shor. 1995. Scheme for reducing decoherence in quantum computer memory. *Physical review A* 52, 4 (1995), R2493.
- [27] Aakarshitha Suresh, Abdullah Ash Saki, Mahababul Alam, Rasit Onur Topaloglu, and Swaroop Ghosh. 2021. Short paper: A quantum circuit obfuscation methodology for security and privacy. In *Proceedings of the 10th International Workshop on Hardware and Architectural Support for Security and Privacy*. 1–5.

- [28] Si-Hui Tan, Joshua A Kettlewell, Yingkai Ouyang, Lin Chen, and Joseph F Fitzsimons. 2016. A quantum approach to homomorphic encryption. *Scientific reports* 6, 1 (2016), 33467.
- [29] Wei Tang, Teague Tomesh, Martin Suchara, Jeffrey Larson, and Margaret Martonosi. 2021. Cutqc: using small quantum computers for large quantum circuit evaluations. In *Proceedings of the 26th ACM International conference on architectural support for programming languages and operating systems*. 473–486.
- [30] Mingsheng Ying, Yuan Feng, and Nengkun Yu. 2013. Quantum Information-Flow Security: Noninterference and Access Control. In *2013 IEEE 26th Computer Security Foundations Symposium*. 130–144. doi:10.1109/CSF.2013.16